Investigations of Air Quality Aspects with the Urban Climate Model PALM4U

R. Wegener, U. Javed, R. Dubus, and D. Klemp

JÜLICH
Forschungszentrum

Schriften des Forschungszentrums Jülich
Reihe Energie & Umwelt / Energy & Environment   Band / Volume 622

Investigations of Air Quality Aspects with the Urban Climate Model PALM4U

R. Wegener, U. Javed, R. Dubus, and D. Klemp

Table of Contents

1 Overall objective of the project

1.1 Embedding of subproject TP6 in phase 1 of the funding program

The funding measure "Urban Climate in Transition", announced by the German Federal Ministry of Education and Research (BMBF) on March 4, 2015, sets itself the task of providing large cities and urban regions with a scientifically based, practical set of tools to address the problems associated with current and future climate conditions and air pollution. A first phase of the program was launched on June 1, 2016, with a duration of 3 years.

A central goal of the BMBF funding measure was the development, validation, and application of a building-resolving urban climate model for entire cities. The research tasks assigned to subproject B in the first phase consisted of processing existing observational data and developing measurement strategies for new measurements. For this purpose, both long-term observations and intensive measurement campaigns (IOPs) have been carried out with high accuracy and high-resolution instrumentation, which not only allowed a model evaluation of PALM4U, but can also be used directly for applications such as air quality control. Especially for the determination of spatial distributions of relevant trace substances, a newly equipped mobile measurement laboratory was used in subproject 6 with temporally highly resolved measurements of NO, NO_2, O_3, CO, CO_2, NH_3, particle size distribution and number concentration in all eight IOPs in Berlin and Stuttgart. The results of the first phase of subproject 6 (module B) were comprehensively published by us in a monograph [Klemp, Wegener, Dubus, Javed, 2020].

1.2 Relationship of project TP6 to the funding policy objectives of phase 2 of the joint project

During the second phase of the funding measure, the overarching goals continued to be achieved through the three modules of the first phase, in accordance with the BMBF's specifications. As Figure 1 shows, the model infrastructure referred to as *PALM4U Workbench* is at the center of the research and development work of the three modules.

The tasks of module B were carried out by the joint project 3DO+M "Three-dimensional observation and modeling of atmospheric processes in cities". On the one hand, the long-term observations (LTO) carried out in phase 1 were continued and special measurements for the evaluation of PALM4U were performed. On the other hand, the model evaluation of PALM4U was carried out both in general and application-specific terms, and Modules A and C were supported by special measurements. A total of 12 Module B subprojects were involved in the evaluation and scientific use of the PALM4U urban climate model in Phase 2 of the [UC][2] funding measure (see Table 1).
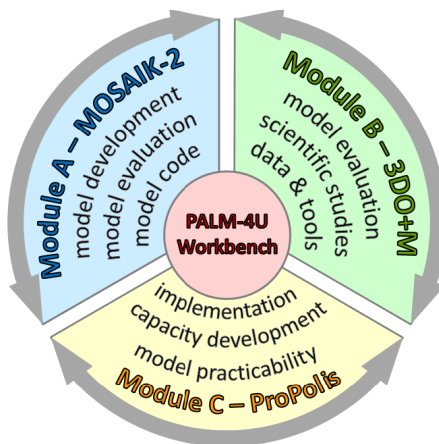
Figure 1 Module structure and scope of the BMBF funding measure "Urban Climate in Transition, Phase 2".

Table 1 Subprojects (TP), scientific management, and applicant institutions in the joint project 3DO+M of module B.

TP	Scientific management	Institution
TP1	**Prof. Dr. Dieter Scherer**	TU Berlin
TP2	Prof. Dr. Christoph Schneider	HU Berlin
TP3	Prof. Dr. Uwe Ulbrich	FU Berlin
TP4	Prof. Dr. Stephan Weber	TU Braunschweig
TP5	Thilo Erbertseder	DLR
TP6	*Dr. Dieter Klemp and Dr. Robert Wegener*	*FZ Jülich*
TP7	Dr. Bianca Adler and Dr. Christopher Holst	KIT
TP8	Dr. Ulrich Vogt and Dr. Rayk Rinke	Uni Stuttgart
TP9	Dr. Valeri Goldberg	TU Dresden
TP10	Prof. Dr. Felix Ament and Prof. Dr. Bernd Leitl	Uni Hamburg
TP11	Dr. Andreas Philipp and Dr. Christoph Beck	Uni Augsburg
TP12	Prof. Dr. Günter Groß	Uni Hannover

Forschungszentrum Jülich worked on sub-project 6 of module B. The work carried out was concerned with the "Investigation and processing of air quality aspects within the framework of the further development of the PALM4U urban climate model". In detail, TP6 dealt with the following topics:

1.3 Processed topic packages

1. *Provision of vehicle emission data for PALM4U in the context of special measurements*

2. *Determination of the heterogeneity of urban pollutant concentrations by mobile measurements with second resolution*

3. *Model studies on local ozone formation based on recent precursor studies*

4. *Urban-surrounding studies*

5. *PALM4U model evaluations*

6. Use of PALM4U in own applications

2 State of science and technology; previous work

The governmental immission monitoring in Germany is based on a network of fixed measuring stations, where the regulated pollutants are continuously on an hourly basis. For the detailed evaluation of the chemistry module of PALM4U and the exploration of its full capabilities, these data sets are only suitable to a limited extent, since a comprehensive evaluation on a city scale level requires both a high time resolution and a comprehensive data set of chemical supporting parameters. In recent years, Forschungszentrum Jülich has set up a mobile measurement laboratory called "MobiLab", which fulfills the above-mentioned requirements and, moreover, is capable of not only point-by-point but even area-based comparisons with the model results.

2.1 Previous work of the applicants

Our working group has been involved in the past and is currently involved in several national and international projects on the composition of anthropogenic emissions and the description of air quality: 1996 - 2000 BMBF project EVA: (Evaluation of Emission Calculation Models) [Klemp, 2002] 1998 - 2004 Participation in the BMBF lead project MOBINET (Mobility in the Munich Agglomeration) 2011 - 2013: Participation in the EU project PEGASOS (Pan-European Gas-AeroSols-climate interactiOn Study) [Ehlers, 2014]; Since the end of 2013: Investigations on the polluter situation for NO_x and particulate matter in the city of Bad Homburg, [Ehlers et al., 2016a]; Since the beginning of 2015: BMWi project ALASKA: Climatology of trace gas concentrations in traffic-loaded areas (highways, inner cities, tunnels), quantification of the occurring load peaks and continuous loads, design of the filter capacity to protect the fuel cell in continuous operation as an automotive drive system [Talke et al., 2018] [Klemp et al., 2021].

2.2   The mobile measurement laboratory of FZ Jülich (MobiLab)

The IEK-8: Troposphere has been operating a mobile measurement laboratory (MobiLab) for several years, whose temporally highly resolved gas and particle phase analysis has been continuously expanded [Ehlers, 2014; Ehlers et al., 2016b; Klemp et al., 2012; Urban, 2010; Wenk, 2016]. Figure 2 describes the basic setup of the measurement system. The vehicle can be used to record the main gaseous and particulate pollutants along with meteorological parameters while driving with a high temporal resolution of one second for most of the parameters.

While other mobile measurement vehicles have been described in the literature, they have limited analytics for measuring selected trace substances or parameters (e.g., VOCs [Coggon et al., 2018] aerosols [Schneider et al., 2008], meteorological parameters [Belusic et al., 2014]. Another unique feature of our project is the linking of the high temporal resolution measurements with the high-resolution model PALM4U. A literature and patent search (Scifinder) conducted by Forschungszentrum Jülich could not find any publication on simultaneous high-resolution mobile measurements of CO_2, pollutant gases and aerosols in inner cities.
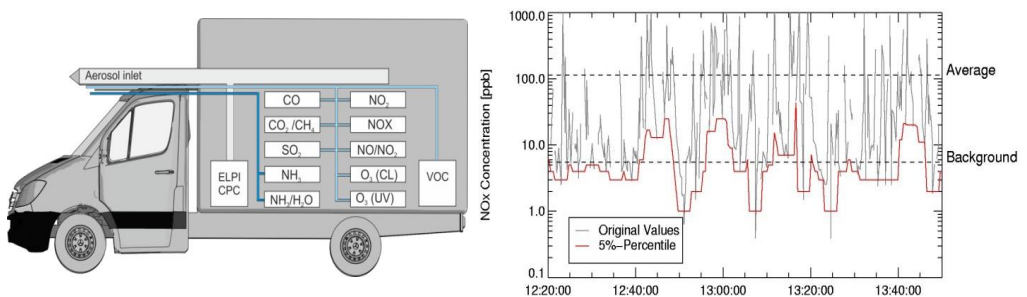

Figure 2 Left: MOBILAB of FZ Jülich is equipped with high temporal resolution gas phase and particle phase as well as meteorological analytics. Right: Berlin, August 2014, measurements in Neukölln with MOBILAB's NO_x analytics: Original values of NO_x vary between approx. 10 and 1000 ppb on a time scale in the seconds range.

3 Results

3.1 Provision of vehicle emission data for PALM4U

The results of our mobile tunnel measurements during project phase 1 have shown that the emission factors used in the literature are inadequate in some cases, as they do not adequately reflect the emission behavior of the current vehicle fleet. In order to keep vehicle emissions as input data up to date, the study on emission factors in the Heslacher Tunnel in Stuttgart that started in 2016 was needed to be continued. For the second phase, the setup of MobiLab was expanded with additional analytics so that now also highly resolved measurements of formaldehyde and N_2O could be provided. Formaldehyde (HCHO) plays a central role in atmospheric chemistry as a source of radicals and accelerates photochemical processing in an air mass. The increasing importance of road traffic as a source of emissions of the climate gas N_2O has already been pointed out [Klemp et al., 2020].

3.1.1 Continuation of the tunnel studies in the Heslacher Tunnel

The tunnel studies started in 2016 to determine the emission factors of gaseous and particulate emissions of the current vehicle fleet. Results of the first phase of the founding period showed that the Heslacher Tunnel in Stuttgart (cf. Fig. 3) is particularly suitable for emission studies.

- The Heslacher Tunnel connects the Stuttgart freeway interchange with the B14, which runs directly through Stuttgart, and therefore has an extraordinarily high traffic volume (throughput: approx. 50000 vehicles/weekday, including 2500 trucks).
- With a length of approx. 2300 m, it has a sufficient length so that atmospheric trace substances (in this case ozone) introduced by vehicle-induced turbulence do not have any noticeable effects on the distribution of nitrogen oxides.
- The changing load situations (constant speed conditions outside rush-hour times, stop-and-go conditions during rush-hour times) allow the investigation of different emission conditions of the current vehicle fleet.

- The good traffic accessibility of the tunnel allows a high frequency of tunnel passages with the measurement vehicle.

Figure 3 presents the results of our emission tests of the current vehicle fleet. Over the entire measurement day, the Heslacher Tunnel was traversed with our mobile measurement laboratory in both directions of travel. Thereby, the temporal course of the trace substances has two maxima (double peaks) at each round trip, since the concentration in the middle of the tunnel is reduced by the supply of fresh air from an additional tunnel entrance.
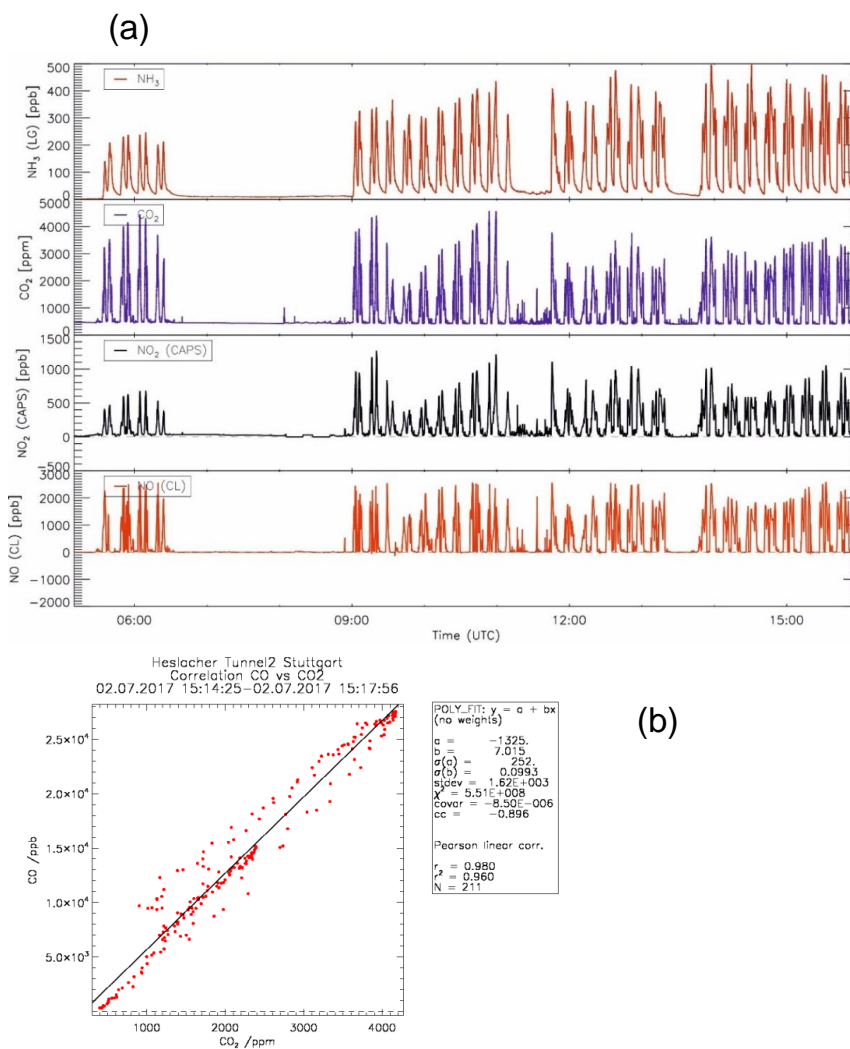
Figure 3 (a) The time series of NH_3, CO_2 NO_2 and NO are shown from an intensive measurement day (08/01/2020) with frequent passages through the Stuttgart Heslacher Tunnel as indicated by extremely large concentrations. (b) Correlation analysis for the determination of the mean trace substance/CO_2 - ratio for a passage through the Heslacher Tunnel.

Investigations on the emission composition of the current vehicle fleet are of particular relevance for the quality of the model results of emission scenarios by PALM4U. An important application is the model-based investigation of different emission reduction measures. Therefore, knowledge of the emissions and their error ranges is essential for assessing the significance of the determined reduction potentials.

The source attribution of tunnel measurements is particularly easy since the pollutants here clearly originate from the traffic. In addition to the trace gases shown in Fig. 3, the trace substances CO, HCHO, SO_2 and N_2O, the particle number as well as the particle size distributions, methane, and VOCs (C_2 - C_{17}) were measured with the extensive measurement analytics of the MobiLab in summer 2020. The normalization of the trace substance concentrations measured in the tunnel to the simultaneously measured CO_2 concentration curves (i.e. fuel consumption) corrects for changing traffic densities and ventilation conditions in the tunnel.

Table 2 lists the mean trace contaminant/CO_2 ratios measured in 2017 and 2018 and compares them to the corresponding ratios for summer 2020.

Table 2 Comparison of trace gases/CO_2-ratios from the Heslacher Tunnel between the mean values of the results of the 2017 and 2018 urban climate I campaigns with those of summer 2020.

Trace gases (TG$_i$)	Heslacher Tunnel Mean 2017 and 2018 TG$_i$ / CO_2 [ppb/ppm]	Heslacher Tunnel Mean Summer 2020 TG$_i$ / CO_2 [ppb/ppm]
CH_4	0.00012	0.00013
CO	4.5	3.8
NO	0.99	0.70
NO_2	0.48	0.19
NO_x	1.47	0.89
NH_3	0.06	0.11
SO_2	0.0085	0.0035
HCHO	---	0.012
N_2O	0.055[2]	0.06

The following conclusions can be drawn from the results listed in Table 2:
- Motor vehicle traffic remains an insignificant source of methane.
- NH_3 is the only trace gas for which a substantial increase of nearly a factor of two is observed within about two years.
- Reductions within the study period, on the other hand, were observed for nitrogen oxides (- 40 %), CO (- 15 %) and SO_2 (- 60 %).
- For N_2O, the emission factor normalized to CO_2 remained almost constant.

[2]N_2O measurements were done in winter 2018 only. Due to the strong dependence on the formation conditions in the catalysts (increased N_2O emissions occur with strong temperature changes), the values are only comparable to a very limited extent.

- In good agreement with the trends given in Table 2, there were increases in the NH_3/NO_x ratio from about 3 % [ppb/ppb] to 9 % for the study period from 2017 - 2020. The obvious reason for this rapid increase is the increasing share of EURO-6 Diesel vehicles with SCR cats and the resulting NH_3 slip associated with the nitrogen oxide reduction measures of diesel engines.

3.1.2   Studies on the temperature dependence and weekday/weekend dependence of the emission behavior

Looking at the seasonal behavior of the CO_2-normalized nitrogen oxide emissions, a clear temperature trend becomes apparent (Fig. 4): CO_2-normalized NO_x emissions measured in the Heslacher Tunnel increase by about 40% from summer to winter. Further the NO_x emissions on weekdays are relatively larger compared to the weekends, as shown by the NO_x/CO_2-ratios (Fig. 4). A simple link with the automatic traffic counts conducted at the tunnel portals[3] and the proportions of cars, light commercial vehicles, and trucks reported there demonstrates the importance of trucks for NO_x emissions.

---

[3] The authors thank David Geyer and Marlene Picha, Landeshauptstadt Stuttgart, Amt für öffentliche Ordnung, Integrierte Verkehrsleitzentrale (IVLZ) for providing the data.
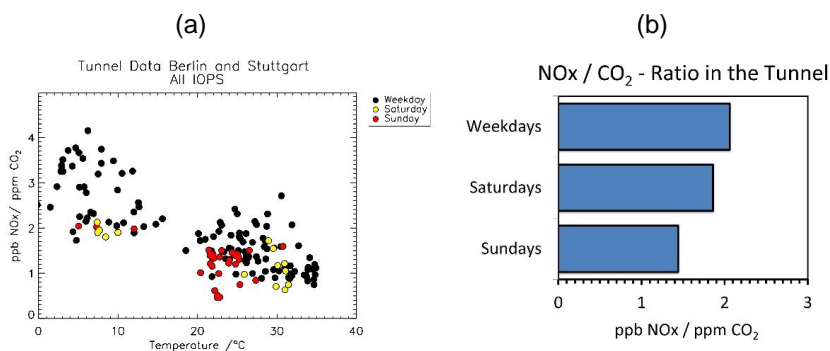
(a)   (b)

Figure 4 (a) Temperature dependence of NO_x/CO_2 ratios measured in the Heslacher tunnel, sorted by weekdays. (b) Mean NO_x/CO_2 ratios separated by weekdays, Saturdays, and Sundays.

Fig. 5 describes the mean weekly trend of the proportions of light and heavy commercial vehicles. On weekdays, both the shares of light and heavy commercial vehicles are almost constant at about 4% each. On weekends, their shares decrease significantly, with Sunday having a commercial vehicle share of only 2%.
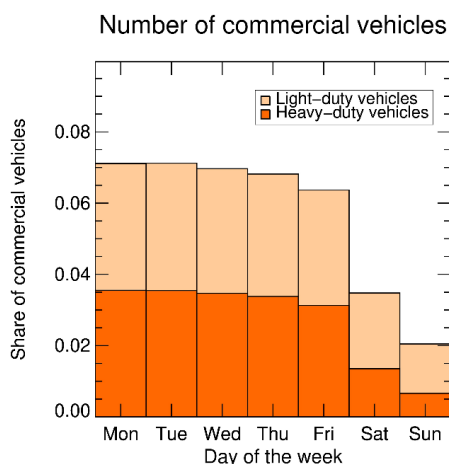

Figure 5 The mean share distribution of light and heavy commercial vehicles in the traffic volume of Heslacher Tunnel (Integrierte Verkehrsleitzentrale (IVLZ), Amt für öffentliche Ordnung, Landeshauptstadt Stuttgart) is shown as a function of the day of the week.

The combination of car and commercial vehicle shares with the NO_x/CO_2 ratios measured (Fig. 4 b) provides the NO_x share distributions for the three modes of transport considered (cf. Fig. 6). On weekdays, more than 50 % of the NO_x emissions measured in the tunnel originate from trucks and light commercial vehicles.

3.2 Determination of the heterogeneity of urban pollutant concentrations by mobile measurements with high time resolution

Subproject 6 carried out two special measurement campaigns in the Stuttgart area with the Jülich measurement laboratory "MobiLab" during the reporting period. The main objective of these special measurements was to continue the long-term study of inner-city air quality that was started at the beginning of the City Climate I phase. The main focus of the investigations was the high-resolution description of the trace substance (TS_i) / CO_2 ratios with i = NO, NO_2, NH_3, CO, O_3, CH_4, particle number and particle size distributions, N_2O, and SO_2.

Furthermore, a recording of the summertime background trace substance pollution downwind of the city (Stuttgart) was carried out during several measurement runs in each case. In addition, for the upcoming evaluations of the air chemistry module implemented in PALM4U, an extensive number of VOC samples (about 60 individual samples per campaign) was taken and analyzed gas chromatographically for their C_2 - C_{11} VOC content in the Jülich laboratories. During the special measurements in
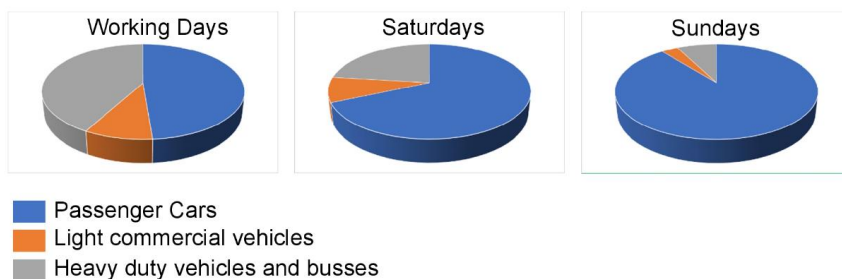
2020 and 2021, we additionally used a sensitive detection method based on absorption

Figure 6 Mean fraction distribution of NO_x emissions in the Heslacher tunnel for working days and weekend days.

tubes to detect higher VOC components (C_9 - C_{17}), so that it was now possible to record practically the entire spectrum of high- and low-volatile organic substances. Together with the nitrogen oxide measurements performed in parallel, this data set allows a sensitive test of the emission and air chemistry module of PALM4U for different radiation conditions. Moreover, this data set forms the basis for comparing the local photooxidant formation determined by PALM4U with that of a comprehensive explicit box model (MCM 3.3.1).

Fig. 7 shows for one working day in summer 2020 (04.08. 2020, 5:30 - 6:57 UTC) the NO_2 concentration course during the MobiLab measurement run in the Stuttgart basin. The highest NO_2 values are observed around Stuttgart's main road E14.
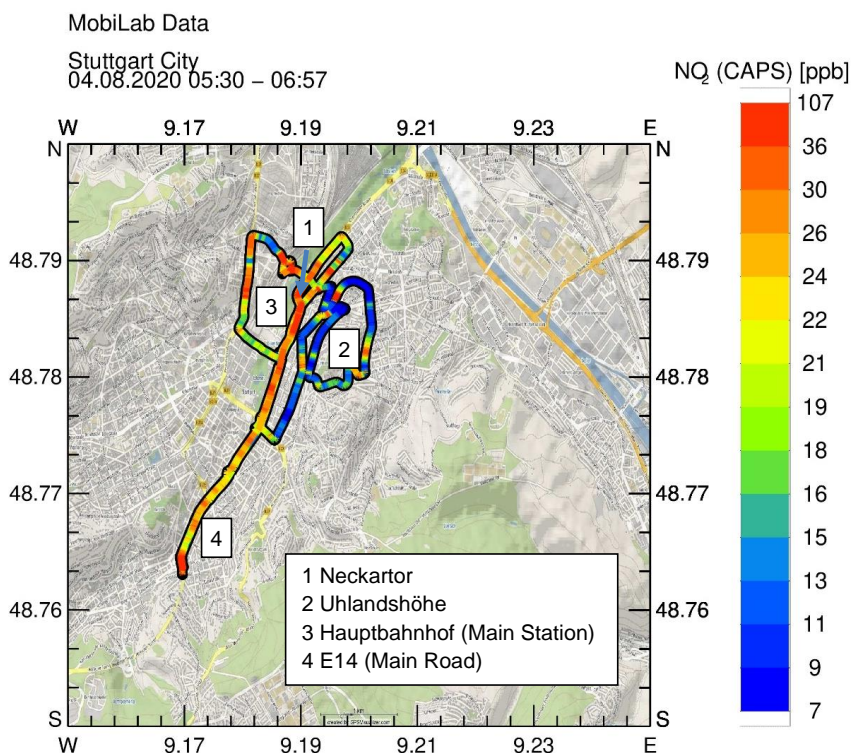

Figure 7 NO_2 concentration course for a working day in summer 2020 (08/04/2020, 5:30 - 6:57 UTC) during a MobiLab measurement drive on the standard measurement route in the Stuttgart basin.

Up to an order of magnitude lower NO_2 concentrations were measured by us in the residential area of Uhlandshöhe, which is only a few hundred meters away from the E14, a circumstance that underlines the strong heterogeneity of trace substance distributions within the city.

In addition to the distance to the main roads, traffic density and meteorological effects such as wind direction and wind speed as well as inversion effects have to be considered as further decisive influencing factors[4] for the level of NO_2 concentration.

3.3 Model studies on local ozone formation based on actual precursor investigations

Parallel to the recorded NO_2 and NO_x concentration courses, numerous VOC samples were taken and analyzed during the measurement campaigns. For the air-chemical interpretation of the results with respect to their photooxidant formation capability, a reactivity consideration of the precursor substances offers decisive advantages: More than 90% of all VOCs in the atmosphere react with atmospheric OH radicals. Therefore, the atmospheric processing of an air mass can be described in good approximation by the total turnover of VOCs with OH (total reactivity R_{VOC}). The composition of the VOC mixes found therefore allows a transformation of the concentration of VOC_i into its respective VOC reactivity R_{VOC} with respect to OH. The OH reactivity describes the turnover rate of an individual VOC with OH radicals and which is equal its concentration $[VOC_i]$ multiplied with its reaction rate constant towards OH k_{OH+VOC_i} (cf. 1). The summation of all VOCs then yields:

$$R_{VOC} = \sum k_{OH+VOC_i} \times [VOC_i] \tag{1}$$

The reactivity parameter is extremely useful because it allows the description of the local ozone production for VOC mixtures of different compositions using a single parameter (cf. [Klemp et al., 2012]).

---

[4] The influence of the diurnally varying inversion height on the NO_2 concentrations has already been presented in detail in [Klemp et al., 2020, figure 14].

Fig. 8 shows typical VOC compositions in terms of the relevant OH-reactivities for the measurement locations Hauptbahnhof and Uhlandshöhe. Additionally, a typical VOC composition for a "background" VOC mix is shown for comparison.
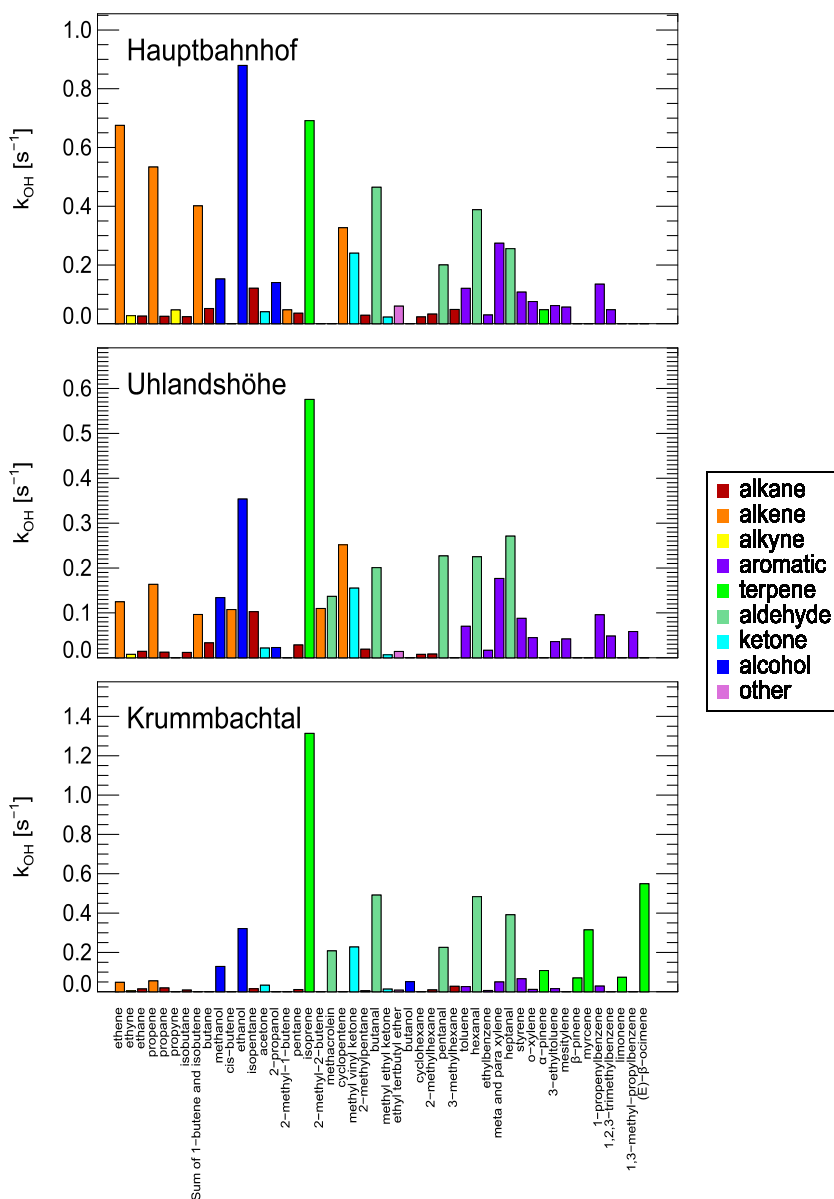
Figure 8 Typical VOC pattern under near-traffic conditions (Hauptbahnhof); Typical VOC pattern of a Stuttgart residential area (Uhlandshöhe) and a VOC pattern of a windward background area (Krummbachtal) with biogenic influence. The different VOC classes are marked in color. Note: For better comparability, all VOC patterns were normalized to a total reactivity of 10 s^{-1}.

The comparison of the VOC pattern at the traffic-dominated "Hauptbahnhof" with that of the residential area "Uhlandshöhe" shows remarkable differences:

- At "Hauptbahnhof", the reactivity fraction of reactive alkenes emitted mainly by traffic were about three times higher than in the residential area.
- The aromatics fractions hardly differed between "Hauptbahnhof" and "Uhlandshöhe", which can be attributed to their substantially higher atmospheric lifetime with respect to OH radicals compared to alkenes.
- In both urban patterns, a similar signature of higher aldehydes was found, which are at least partly generated during VOC processing. The significantly higher aldehyde fraction at the "Hauptbahnhof" shows that a substantial fraction of aldehydes was also emitted directly.
- The similarly high proportion of biogenically emitted isoprene, a hydrocarbon with an atmospheric lifetime of only 15 - 30 min, at both urban sites is noteworthy. This reflects the clear influence of biogenic emissions from the surrounding park areas also in the "Hauptbahnhof" area.
- The comparison with a VOC background pattern from the upstream "Krummbach" valley underlines the even higher influence of biogenic VOC sources here: In addition to isoprene, significant proportions of terpenes were also found here. Alkenes and alkanes, on the other hand, had only a small share of the reactivity budget under background conditions.
- The city center (Hauptbahnhof) is also a significant source of alcohols, the concentration of which is about a factor of two higher here than in the residential area at "Uhlandshöhe".

In atmospheric processing, the VOC and NO_2 compete for OH (cf. Fig. 9). Ozone is formed only after the reaction of VOC with OH (R_{VOC} reaction path) on the R_{NO2} reaction path, the nitrogen oxides present in the form of NO_2 are converted to HNO_3 and removed from the atmosphere by leaching processes. The ratio of R_{VOC}/R_{NO2} reactivities controls the relative importance of the two processes in trace substance removal. In Fig. 9, these processes are shown in a simplified scheme of the trace substance degradation of VOC and NO_2 in the troposphere.
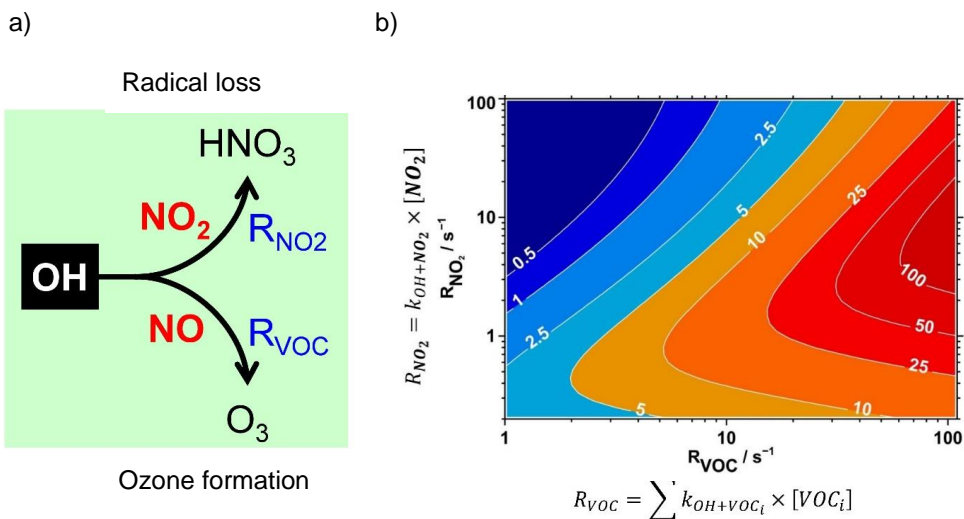
a)   b)

Figure 9 (a) A simplified scheme of the reaction pathways of OH radicals in the trace substance degradation of nitrogen oxides and VOCs. Only the R_{VOC} reaction pathway forms additional ozone in the atmosphere; the R_{NO2} reaction pathway converts nitrogen oxides present in the form of NO_2 to HNO_3, which is removed from the atmosphere by leaching processes. The ratio of R_{VOC}/R_{NO2} reactivities controls the relative importance of the two processes in trace substance removal.

(b) Result of variational calculations with MCM-3.3.1 (details: see [Ehlers et al., 2016b; Klemp et al., 2012]), where for different starting ratios and starting reactivities of VOC and NO_2 the resulting ozone production rates are shown as a so-called $P(O_3)$-isopleth plot of local ozone formation. Radiation conditions: 06/21, noon 12:00 local time. A rapid conversion between NO and NO_2 occurs at noon over the photostationary state on the time scale of 1 - 2 minutes.

Using a detailed reaction model (MCM, Master Chemical Mechanism [Jenkin et al., 1997]), the photochemical impact (i.e., photooxidant formation) can be studied for different initial R_{VOC}/R_{NO2} ratios. The main advantage of this approach is that for the measured input parameters (NO_2, VOC-mix, radiation data), the description of photochemical ozone formation valid for that location can be used. The upper left region of the isopleth diagram is characterized by small VOC/NO_2 ratios typically found for urban areas of Central Europe. An increase in VOC reactivity leads to an increase in ozone production. Accordingly, this area in the isopleth plot is called <u>VOC-limited</u>. An increase in NO_2 concentration, on the other hand, causes a decrease in ozone production. The reason for this is that at high NO_2 concentrations the reaction

of NO_2 with OH starts noticeably to compete with the decomposition of VOCs by OH. The optimum of ozone formation is therefore reached when the VOC/NO_2 ratios are just such that, on the one hand, sufficient reactive VOCs and sufficient NO are available to generate a new generation of OH radicals from HO_2 and RO_2 radicals, but, on the other hand, the OH radicals are not lost again too quickly due to excessively high NO_2 concentrations.

In contrast, large VOC/NO_2 ratios characterize the lower right region of the isopleth plot. This air chemistry scenario is typical for rural regions far from the source, since during the transport of an air mass, nitrogen oxides are removed from the atmosphere faster on average by OH radicals compared to VOCs. Moreover, rural regions in particular form a significant source of biogenically formed hydrocarbons, so that VOC/NO_2 ratios also increase. In this region of the isopleth plot, the slope of the $P(O_3)$ isopleths is positive with increasing NO_2 reactivity. An increase in NO_x concentrations also leads to an increase in ozone formation; therefore, this portion of the plot is referred to as the <u>NO_x-limited</u> region. If the NO_x concentration is decreased further, the system does not contain enough NO_x to recycle the OH radicals sufficiently fast by radical reactions with NO.

Fig. 10 shows the VOC and NO_2 reactivities[5] of the individual samples measured during the summer in Stuttgart:

- It can be seen that the vast majority of samples cluster around the range of about 10 s^{-1} R_{VOC} and 10 s^{-1} R_{NO2}. This corresponds to typical inner-city concentrations of traffic-influenced areas found in Stuttgart.

- A number of samples with rather higher R_{VOC} values and lower R_{NO2} values were also found. These sampling sites are urban background samples, (sampled e.g. near a park).

- For a rough classification of the summertime (R_{VOC}/R_{NO2}) ratios obtained in Stuttgart, the processing and dilution curves taken from [Ehlers et al., 2016b] are plotted. They describe the behavior of an air mass moving from the source location "congested inner city" to the rural background areas in 1994 and around 2014,

---

[5] The input NO_2 reactivities of the samples were calculated from the measured NO and NO_2 values after setting the photostationary equilibrium, $J_{NO2} = 0.0084$ s^{-1} and assuming an ozone concentration of 50 ppb.

respectively. Since over the course of the last two decades a much stronger reduction of VOCs occurred than for nitrogen oxides, a typical air parcel from 1994 started in a city with much higher ozone formation rates. As it was transported out of the city, the imaginary air parcel, on its way from the source location to the background areas, swept over regions in the isopleth plot with much higher ozone formation rates than 20 years later. This fact is consistent with the observation of a steady decrease in peak summer ozone levels over the past two decades.

- Therefore, considerably less ozone formation occurs in cities nowadays than two decades ago.
- It is noticeable that the peak of summertime inner-city (R_{VOC}, R_{NO2}) ratios measured in Stuttgart occurred at lower R_{NO2} values and higher R_{VOC} values than the starting point of the 2014 processing and dilution curve.

Two circumstances can be considered as obvious reasons:

- First, in the Ehlers et al. paper, we used seasonal averages to calculate the starting value for 2014 of VOC reactivities for which the additional biogenic contribution is small. As shown by us in Fig. 8, this effect is by no means negligible for daytime summer VOC reactivities, even for areas close to traffic.
- Second, over the past several years, inner-city NO_x reactivity has steadily decreased. This is reflected in the lower R_{NO2} starting values.
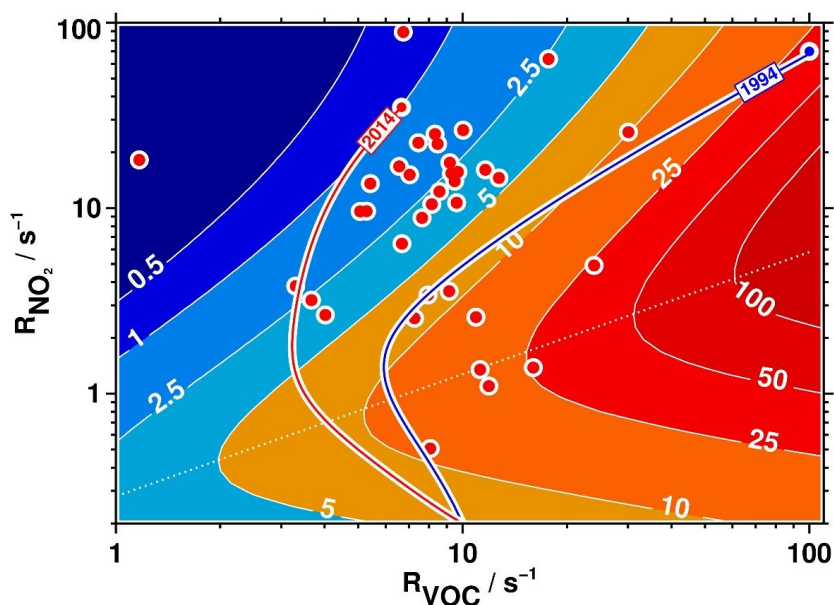
Figure 10 Presentation of summertime inner-city (R_{VOC}, R_{NO2}) conditions measured in Stuttgart during the 2017 and 2018 IOP's and characterization of their potential ozone formation. Boundary conditions for the isopleth plot shown: Stuttgart, 6/21, 12:00 p.m. Plotted is the mean processing and dilution curve of a hypothetical air parcel during transport from the inner city in 1994 and 2014 from [Ehlers et al., 2016b].

For a comparison with the results of the summer measurement campaign, the processed results from IOP III (winter 2017/2018)[6] were used. The comparison of the winter (Fig. 11) with the summer isopleth plot (Fig. 10) shows that under clear-sky conditions significant ozone formation also takes place in winter. It reaches about 25 – 30 % of the summer ozone formation rates under optimal (R_{VOC}/R_{NO2}) conditions.

Unlike in summer, a wide range of variation of about a factor of 5 in the measured (R_{VOC}/R_{NO2}) ratios was observed for both R_{VOC} and R_{NO2}. The obvious explanation for this effect is the exceptionally frequent occurrence of wintertime inversions, which reduce dilution of traffic emissions by convective processes. Support for this hypothesis is provided by the fact that the same dilution factor is observed on average

---

[6] This was due to the fact that the planned Stuttgart winter special measurement campaigns had to be cancelled because of the corona-related restrictions.

for both precursor substances (which manifests itself in the double-logarithmic plot of Fig. 11 as a linearly increasing band of observed start reactivities).

In both summer and winter, typical urban (R_{VOC}/R_{NO2}) conditions were in the range of small ozone production rates, so that only few ozone was formed near the sources. It should be noted, however, that the strong reduction in nitrogen oxide emissions as a result of the widespread introduction of SCR cats in diesel vehicles shifts the future start reactivities into photochemically "more active" areas of the isopleth plot, with the consequence that this tends to lead to increased "cumulative ozone production" on the transport path of this air mass from the source areas to the background regions (cf. chapter 3.5.3.2).

However, it can also be seen from Fig. 11 that this effect has little impact on wintertime ozone production, since in winter the lack of biogenic VOC emissions cannot produce a "kink" in the dilution and processing curve" into more photochemically active regions. Unlike under summer conditions, the rate of ozone formation hardly increases during the course of dilution and processing to small R_{NO2} values, since practically no values below R_{NO2} of 1 s^{-1} were observed as a result of the lower winter photochemical activity.
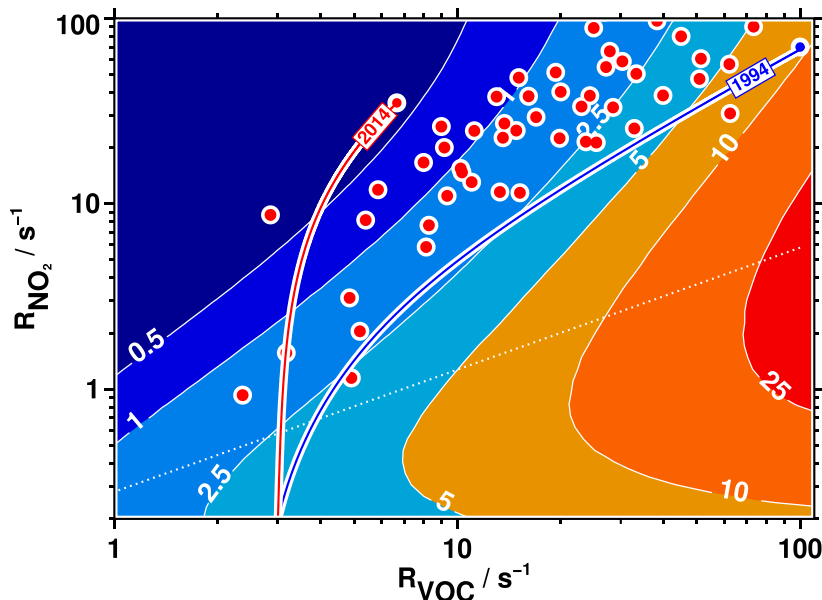
Figure 11 Plot of wintertime inner-city (R_{VOC}/R_{NO2}) conditions measured in Stuttgart (IOP III, winter 2017/2018) and characterization of their potential ozone formation. Boundary conditions for the isopleth plot shown: Stuttgart, 12/21, 12:00 local time. The associated NO_2 reactivities were calculated from the measured NO and NO_2 concentrations after completion of the PSS setting, assuming an ozone concentration of 50 ppb and the winter midday value for J_{NO2}. Additionally, the processing and dilution curves for 1994 and 2014 calculated from [Ehlers et al., 2016b] are plotted. The lack of wintertime inputs of biogenic VOC emissions and the contribution of long-lived VOCs and wintertime elevated CO levels cause the processing and dilution curves to end at a minimum of about 3 s^{-1}.

3.4   Urban-surrounding studies

For the realistic modeling of inner-city trace substance concentrations, both current emission scenarios and the correct description of background concentrations of the substances must be taken into account in addition to the description of the meteorological and air-chemical process sequences. In order to capture the dynamics of the relevant concentration levels, urban-rural studies were conducted over several days during the MobiLab measurement runs. An example of the interaction of the prevailing background concentrations for ozone with the inner-city emission scenario of nitrogen oxides is given in Fig. 12.

3.4.1 On the role of background ozone

Basically, ozone and NO_2 concentrations behave in opposite directions. This is because typical summertime background ozone concentrations of about 40 ppb are found upwind of the city, while on a busy road, advected ozone concentrations are converted to NO_2 with NO emissions emitted by road traffic. This process, named as "ozone titration", leads to a drastic increase in NO_2 levels along with a decrease in the ozone levels close to the traffic. The consequence for inner-city NO_2 concentrations is that their concentration levels are not only controlled by direct emissions, but are also directly correlated with background ozone concentrations, at least as long as NO concentrations are much higher than background ozone concentrations. In the rural forest areas west of Stuttgart, ozone concentrations between 35 and 40 ppb were observed. It is noticeable that the simultaneously measured NO_2 concentrations here had a background value of only about 2 - 3 ppb, on top of which a variable NO_2 fraction of about 8 - 10 ppb was observed. In addition to ozone titration effects due to NO from the exhaust plumes of individual motor vehicles, direct NO_2
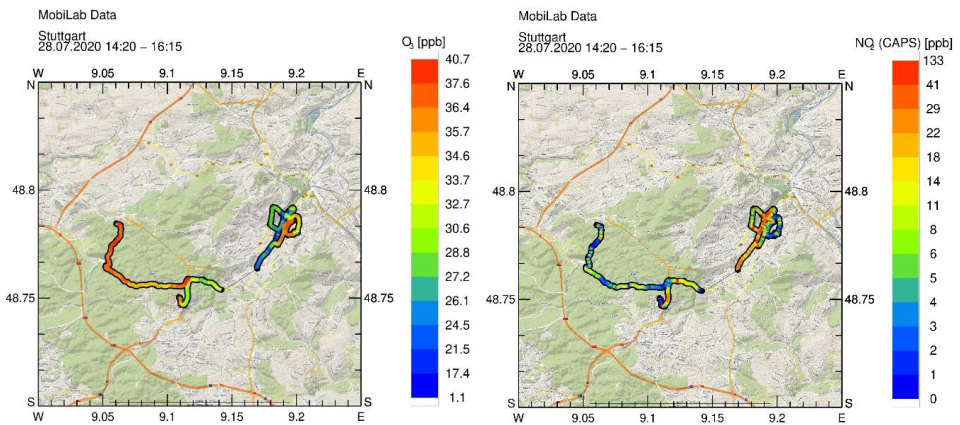
Figure 12 Comparison of the concentrations found for ozone and NO_2 in the Stuttgart basin and in the upstream forest area west of Stuttgart. During the measurement run with start and end point Vaihingen (University), westerly inflow conditions prevailed. The trace substance concentrations measured in the Heslacher tunnel were "masked out" here.

emissions from diesel vehicles[7] with oxidation catalysts are probably responsible for the greater variability of the NO_2 values compared to that of ozone.

3.4.2 Determination of the contribution of biogenically emitted VOCs based on simultaneous VOC and NO_x sampling

Fig. 13 classifies the results of a summer measurement campaign in Stuttgart with respect to their local ozone formation rate as well as their contribution of biogenic VOCs to R_{VOC}.

- Relatively low biogenic fractions (5 - 15 %) of VOC reactivity are observed for inner city samples, recognizable by their high NO_2 reactivities.
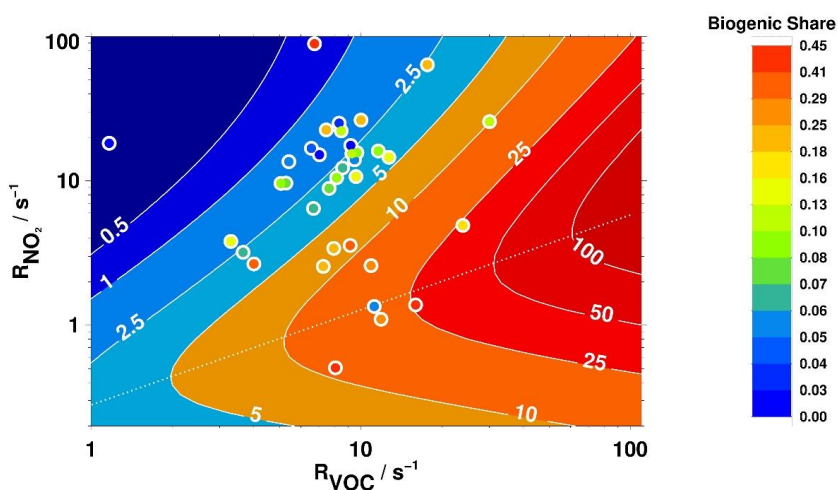
Figure 13 Classification of VOC samples collected during a summer measurement campaign according to their reactivity contribution by biogenically emitted VOC. Shown are the found (R_{VOC}, R_{NO2}) reactivities and their respective positions on the isopleth diagram for summer conditions: (Stuttgart, 06/21, 12:00 local time).

[7] From diesel vehicles with oxidation catalysts at operating temperature, about 20 to 30% of the NO originally released by the engine is converted to NO_2 [see: Klemp et al. 2012].

- Low NO_2 reactivities are characteristic of rural background sampling. A significant increase in biogenic VOC content with decreasing NO_2 reactivity is evident.
- Inner-city samples and samples from the urban background have comparable VOC reactivities on average. Here, in the background samples the decreasing anthropogenic contribution is replaced[8] by an increasing biogenic reactivity contribution.

3.4.3   Cold air flows and urban heat island effects in the Stuttgart area

The basin location of Stuttgart with its orographically structured environment favors the formation of a ground-level local wind system during the summer months [Schädler & Lohmeyer, 1996]. Mainly during meteorological situations with low supraregional wind, a local air exchange is formed during the night hours and in the mornings, during which cooler slope air flows off into the inner-city area via gorge-like valley incisions (mainly through the Nesenbach valley) (cf. Fig. 14 a). This cold air drainage from the

(a)   (b)
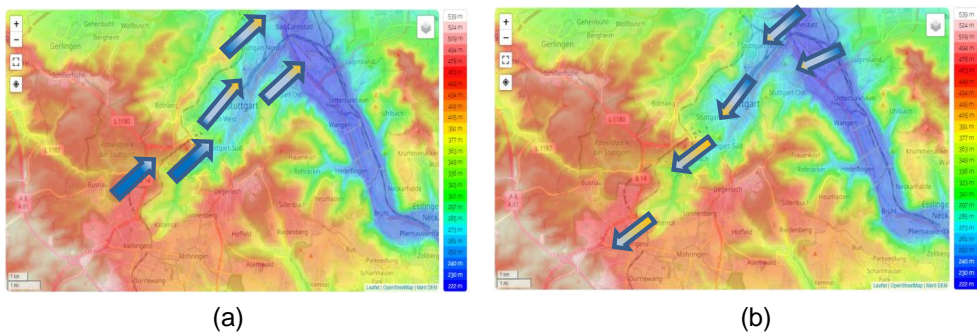
Figure 14 Topographic map of Stuttgart (source https://de-de.topographic-map.com) with Nesenbach valley in southwest-northeast direction and Neckar valley in the northeast of Stuttgart. The basin of Stuttgart leads to the formation of a local wind system. (a) At night: Cold air runoff from the mountains reduces pollution in the Stuttgart basin. (b) During the day: Warm air transports the pollutants from the basin to the mountains.

---

[8] In retrospect, this circumstance additionally confirms the course of the processing and dilution curve shown in Fig. 10 for an air parcel on its way from the source location "city" to a biogenically dominated background area.

mountains not only leads to a noticeable reduction in nighttime temperatures in the city, but also reduces pollution in the Stuttgart basin.

During the day, on days with high levels of radiation, the slope heating of the Nesenbach valley, located southwest of the city, causes an upslope flow. In such situations, this warm air flow effectively contributes to an improvement of Stuttgart's air-hygienic situation since it transports pollutants from the valley basin to the surrounding mountainous regions (cf. Fig. 14 b).

On July 8. and 9. 2018, flights and ground-based investigations of the city of Stuttgart and its surrounding area were carried out within the framework of coordinated investigations. In addition to the acquisition of measurement data sets for the evaluation of PALM4U model calculations, the experimental verification of the above-mentioned local wind system was another goal of this intensive day for us. Fig. 15 is taken from the publication [Samad et al., 2023] and describes the travel and flight routes of different participants (FZ Jülich, MobiLab; DLR, light aircraft Cessna; and DWD, temperature profiles) during the intensive campaign IOP IV in June 2018. On these days, the route of the MobiLab (Fig. 15, blue route) led through the Stuttgart
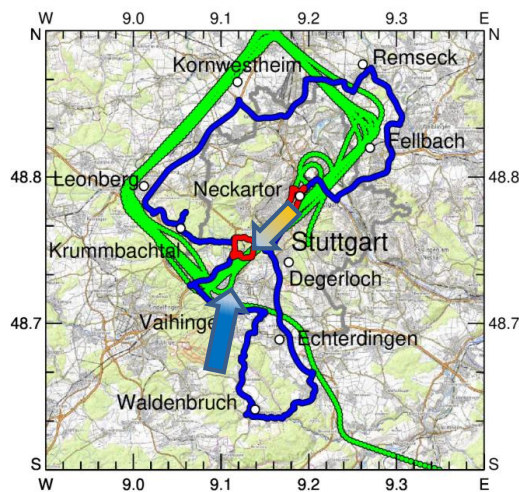
Figure 15 Travel and flight paths of different participants (FZ Jülich, MobiLab; DLR, light aircraft Cessna; and DWD, temperature profiles) of IOP-4; intensive measurements on 8. 7. and 9. 7. 2018. The blue arrow shows the course of the nightly cold air flow into the city, and the orange arrow shows the transport of air out of the valley basin during the day.

valley basin and additionally crossed the northern and southern hinterland of the city. It should be noted that experimental evidence of this local wind system was only possible for the ground-based MobiLab, since the DLR Cessna was far above the wind system occurring only near the ground, even at minimum flight altitude, and the DLR vehicle carried out measurements exclusively in the Stuttgart basin. The evaluations of the intensive campaign IOP-4 (Stuttgart) were carried out by us during the second phase of the funding period and are therefore the subject of this book.

In Fig. 16 the height dependence of CO_2 for the MobiLab measurement runs carried out on 07/08 and 07/09 2018 (travel route see Fig. 15) is plotted. On the abscissa the linearized travel profile and on the ordinate the height above sea level is provided. On both intensive days under summer high pressure conditions, the prevailing supraregional wind was only very weakly pronounced, so that good basic conditions existed for the occurrence of the local wind system searched for. As an indicator for anthropogenic activities, we used the CO_2 concentration measured in each case (which was adjusted for emission peaks) and presented it in the form of the specified color code.

CO_2 is particularly suitable for this purpose, because

- it is an indicator for the course of combustion processes,
- it can be detected precisely (better than 1 ppm/s) and with high time resolution by means of cavity-ringdown detection (this allows "cleaning" of the recorded CO_2 data set by subsequent elimination of individual traffic-borne CO_2 peaks).
- In fact, both days showed a uniform behavior of the measured CO_2 profiles:
- In the early morning hours, highest CO_2 concentrations were measured in the Stuttgart basin and in the upstream areas (CO_2 > 440 ppm). The surrounding mountain ranges in the southern forefield of Stuttgart showed significantly lower CO_2 values with 415 - 420 ppm in the morning.
- At noon, the measured CO_2 concentrations of the Stuttgart basin locations and those of the elevated areas converged. This behavior can be attributed, at least to a large extent, to the local exchange of urban air by downslope cold air flows.
- During the afternoon, the flow direction of the local slope wind systems reversed. Then, the heating of the slopes of the Nesenbach valley caused an outward flow towards the city. With this upslope local wind, polluted air was expelled from the valley basin, resulting in improved ventilation of the Stuttgart urban area. As a

consequence, higher CO_2 concentrations were observed at higher altitudes South of Stuttgart in the afternoon compared to the Stuttgart basin[9].
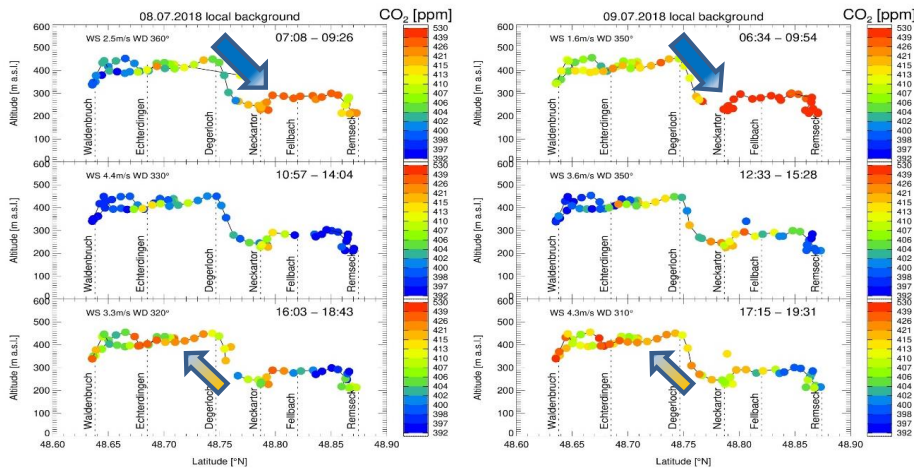
Figure 16 Results of the MobiLab measurement runs (for route see Fig. 15). The linearized driving profile is plotted on the abscissa and the altitude above sea level is plotted on the ordinate. As an indicator for anthropogenic activities, the measured CO_2 concentration was color-coded and adjusted for emission peaks. The course of the measured CO_2 concentrations over the day provides clear indications of the formation of a downslope flow in the morning. In the afternoon, an opposite upslope flow is observed on both measurement days, which also contributes to the better aeration of the Stuttgart basin. The blue arrow shows the course of the nightly cold air flow into the city, the orange arrow the transport of air out of the basin in the afternoon.

[9] The afternoon measurement run also provides an indication that local wind systems, rather than primarily convective processes, are responsible for observed CO_2 behavior. If the increase of the inversion layer height were decisive for the CO_2 behavior, then the CO_2 values in the high-altitude areas should behave analogously to those in the Stuttgart basin in the afternoon (and not, as observed, increase during the day).

3.5 PALM4U-model evaluations

During the funding period, the PALM4U urban climate model was supplemented and extended in numerous respects. From our side, special attention was paid to the evaluation of the newly implemented capability to describe the air chemistry. The following description of the evaluation process of PALM4U, concerning the air chemistry module, explains our approach to evaluate the performance of the newly developed model module[10] .

3.5.1 Analysis of the results of the simple PALM4U chemistry module (photostationary equilibrium) based on VALM01 (Berlin, winter 2017)

In advance, it was decided by the UC[2] consortium that the first evaluation should be performed for a selected period of IOP-1. For this purpose, a PALM4U run for Berlin (VALM01, 17. 01. 2017 UTC - 18. 01. 2017 UTC), whose spatially high-resolution "child" region (model resolution: 1 m) represented the area around Ernst-Reuter-Platz, was performed by the model developers at TU Hannover. This "child" region was embedded into the "parent" model region of the entire Berlin urban area, which was simulated with a coarser resolution. In the first year of the second funding phase, the results of the model calculations from the project module MOZAIK became available and were compared with the VALR01 data set measured during the campaign.

---

[10] It should be noted that the "bugs" we found in the air chemistry module were eliminated by the developers during the second phase of the project. Thus, with the successful run of PALM4U for the Stuttgart intensive phase (VALM04, summer 2018), a functional air chemistry module could be attested for the first time (cf. the corresponding presentation).
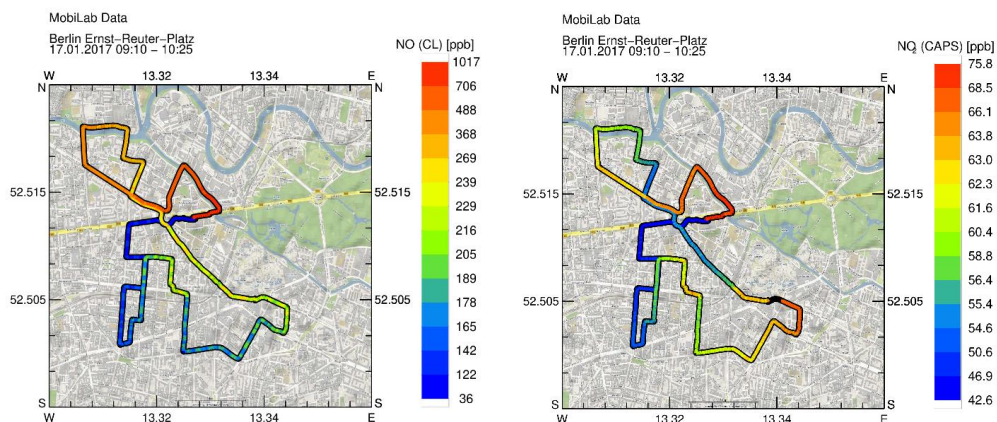
Figure 17 MobiLab trajectory during the first intensive period (VALM01) in the "child" area of Berlin "Ernst-Reuter-Platz. NO and NO$_2$ concentration course during the measurement run 9:10 - 10:25 (UTC) 01/17/ 2017.

NO$_x$-comparisons

Figure 17 shows the concentration curves of NO and NO$_2$ as observed by MobiLab from 9:10 - 10:25 UTC in Berlin during the intensive period VALR01. The output of the PALM4U simulation (Figure 18) was compared[11] to the measured trace substance concentrations. During the evaluation it was found that at the track and the inlet height of MobiLab no output had been provided by the model, due to an error when setting

---

[11] When comparing the measured and modeled NO$_x$ values, it should be noted that MobiLab completed several measurement runs on the measurement route shown in Fig. 17 during 17. 01. 2017 (duration approx. 1 h each), during which particularly high nitrogen oxide values occurred (cf. Fig. 18). For technical reasons, it was necessary to recharge the accumulators between the measurement runs for a duration of 1 - 1.5 h each. During these times, the MobiLab was parked in front of the main building of the Technical University, and the trace gas measurements were also carried on continuously during these time intervals. For the corresponding PALM4U results of these time intervals, the coordinates of the parking position of the MobiLab were used.

up the PALM4U run. Only modeled NO_x values ($NO+NO_2$) from a height of 36 m above ground could be used for the comparison with measurement data. We tried to make the best of the situation. Due to the lack of the modeled 2-m-NO_x-data, we did not only use the measurement data in the street canyons for the comparison, but also the data from measurement stations in the vicinity of Berlin. We had to assume that the NO_x results of PALM4U for a height of 36 m could be approximated with measurements in the background of Berlin rather than with the MobiLab data from the inner city of Berlin. In general, the modeled PALM4U NO_x was governed by emission and dilution effects. During the day, the NO_x values measured at a height of 2 m in the street canyons were much higher than those at the background stations. However, this did not apply at night when MobiLab was in its parking position in front the main building of the TU Berlin offside the street. Here, NO_x concentrations were at a level comparable to the background station values. In the absence of nearby sources the modeled and measured values were at a comparable level (see Figure 18). However, during daytime, measured urban NO_x concentration differed by factor of 4 - 5 from the simulated PALM4U results for 36 m. A more detailed comparison was prevented by the above-mentioned error in the model setup.
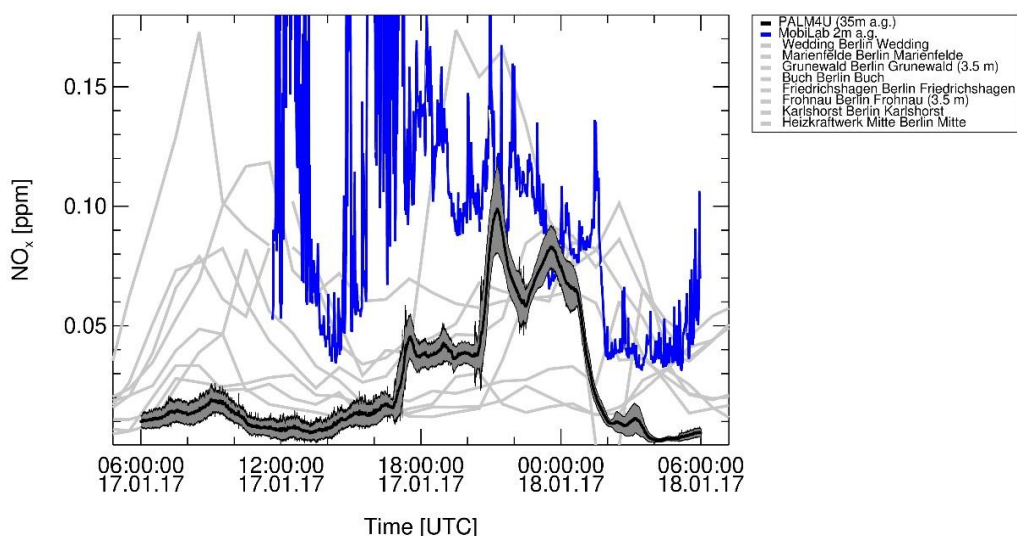
Figure 18 Comparison of modeled (36 m above ground) and measured NO_x concentrations (2 m above ground) for the MobiLab driving course as well as for the intermediate MobiLab standing times in front of the main TU Berlin building (urban background concentration) during the first intensive phase (VALM01) in the "child" area of Berlin "Ernst-Reuter-Platz (spatial model resolution: 1 m). In addition, the NO_x time series from several fixed measuring stations in the surroundings of Berlin were plotted.

Comparison of measured and modelled ozone concentrations

By comparing measured and modeled ozone concentrations, other properties of the PALM4U air chemistry module can be tested, in particular the interaction of regional ozone background concentrations with local nitrogen oxide emissions. While the NO_x comparison focused on the emission term and the efficiency of altitude-dependent dilution of ground-based emissions from traffic, regional emissions and the photostationary equilibrium play key roles in ozone formation.

Unlike nitrogen oxides, atmospheric concentrations of ozone are largely determined by advection from the surroundings. Above the city an almost constant background
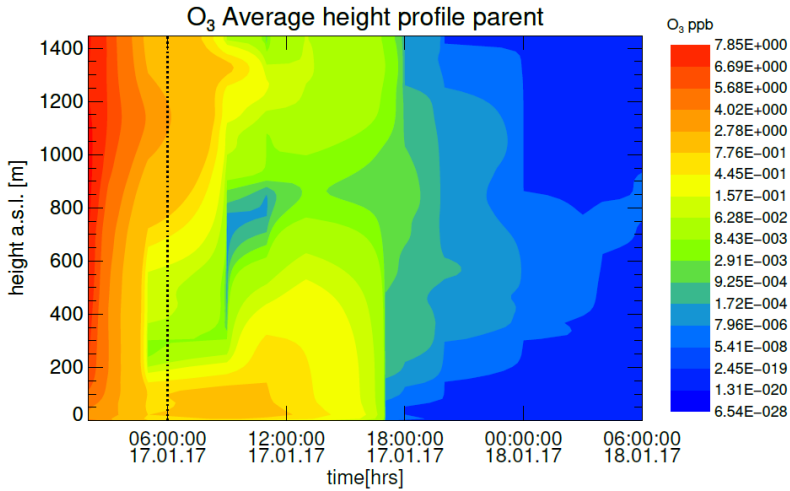
Figure 19 Visualization of the altitude profiles calculated by PALM-4U in the "parent" region for the (VALM01) intensive phase. The dashed line at (01/07/2017 6:00 UTC) marks the beginning of the intensive period VALM01.

ozone concentration will be established. Close to the ground, in the proximity of NO_x sources, ozone will form NO_2 from the reaction with NO.

This process does not lead to a net ozone production, hence the sum of

"Ozone + NO_2 = O_x" remains constant. From Figure 19 it is apparent that in the "parent" domain the modeled average ozone concentration continuously decreased right at the start of the simulation. This effect can be observed at all altitudes. Only on the first day, from early morning to the afternoon, a slight increase in the modeled ozone concentration of few ppb only near the ground was predicted. On the second simulated day, the ozone concentrations in the "parent" region dropped to unrealistic values in the 10^{-10} ppb range.

In order to identify the cause for the low model ozone concentration shown in Figure 19, the O_x/NO ratio from the PALM4U output was plotted as a function of time (cf. Fig. 20).

The chemistry mechanism used for VALM01 contains only the reaction mechanism to describe the photostationary state without additional photochemical ozone production, therefore the quantity $O_x = NO_2 + O_3$ is an invariant. The observed ozone was either advected background ozone or ozone from the photolysis of NO_2. If the ozone was formed from to NO_2 photolysis alone, the O_x/NO ratio would be equal to the NO_2/NO emission ratio (see red line in Figure 20). It was found that in the PALM4U simulation output already at 6:00 UTC almost all of the ozone could be attributed to NO_2 photolysis, as the O_x/NO ratio from the PALM4U simulation (black curve in Figure 20) is almost identical to the NO/NO_2 emission ratio. In contrast to the MobiLab
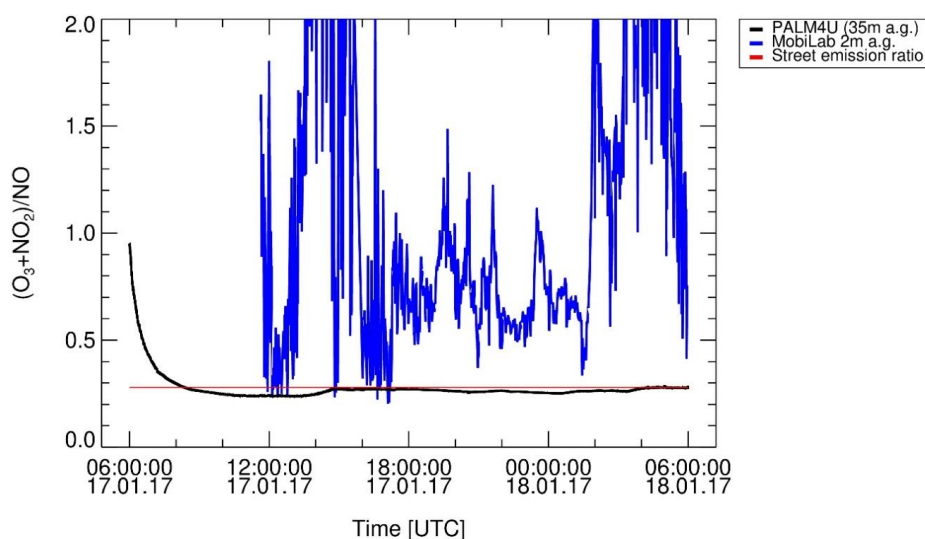
Figure 20 Plot of the modeled O_x/NO ratio (black) and comparison with the modeled NO_2/NO ratio (red) (derived from the emission ratio of nitrogen oxides assumed in the model). Since in the model both quantities are practically identical after a few hours, it can be concluded that the small ozone increase during the day originates exclusively from the photolysis of NO_2. Therefore, in contrast to the MobiLab observations, no contribution from background ozone seems to be present in the ozone increases of the PALM4U model data.

observations (see Figure 12), the contribution of background ozone to the simulated ozone on the second day of the simulation is neglectable.

The reason for both the low ozone concentration on the second simulation day and the low influence of background ozone on the ozone level in the model domain can be found in the setup of the model for VALM01.

Despite the boundary conditions in the simulation mode being set as cyclic[12], chemical species were lost at the outflow of the model domain, due to a failure in the simulation.
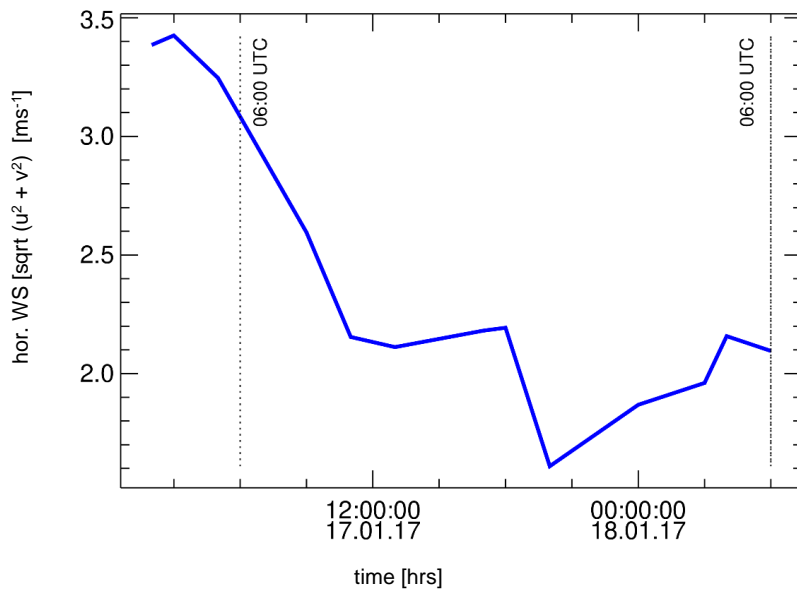
Figure 21 Mean horizontal wind speed (WS) for VALM01 as a function of daytime.

---

[12] In principle, the PALM4U model can be operated with cyclic or non-cyclic mode to balance losses of components that are swept out at the model domain borders. In the cyclic mode, losses of components that leave the model domain on one site enter the model domain on the opposite site again. In the non-cyclic mode components that are lost at the edge of the model domain will be replaced by the results of overarching (regional) models.

In the VALM01 simulations the chemistry of PALM4U was not linked to a regional chemistry model. As a compromise initial values of ozone and other chemical components were specified and PALM4U was operated under cyclic boundary conditions to simulate the background conditions.

The reason for this failure seems to be a lack of continuous inflow of background O_3 from the overarching model domain. As a result, all species moved through the model domain according to the wind direction and velocity in the model and flushed out. To verify this hypothesis, we plotted the time series of the average horizontal wind speed in VALM01 (Figure 21).

The average loss rate of compounds can be determined from the mean horizontal wind speed and the known physical dimensions of the parent domain. Figure 22 shows the simulated ozone concentration time series and the time series resulting from the calculated loss rate.

Especially during the first hours after the start of the model, the simulated ozone time series and the concentration time series calculated solely from the flushout agree[13] very well. Overall, the simulated ozone concentration decreased by more than 6 orders
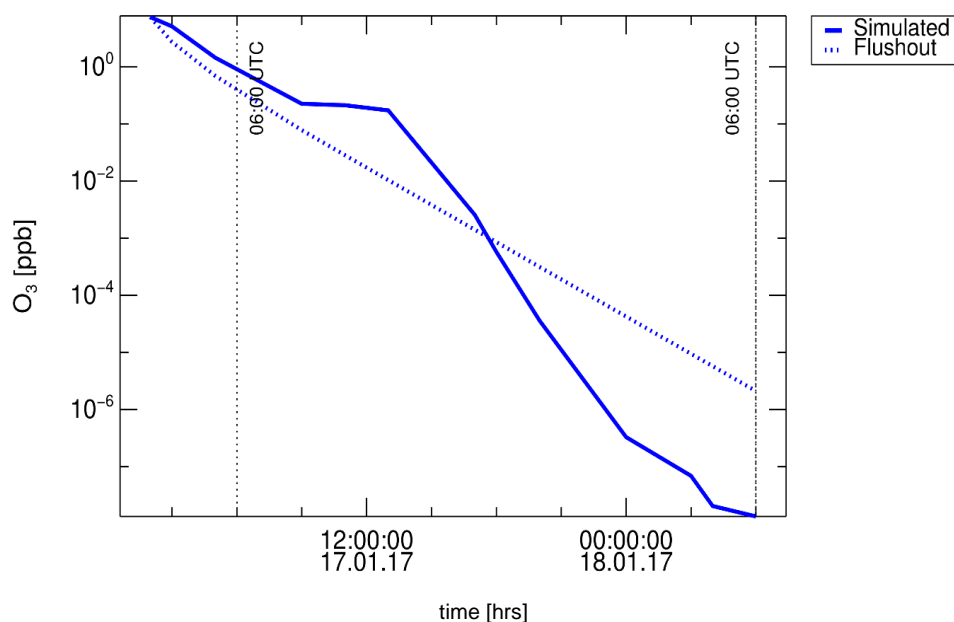
Figure 22 Time series of modeled ozone (solid line) and diluted ozone (dashed line) assuming the flushing rate determined from mean horizontal wind speed and the physical dimensions of the parent domain.

---

[13] During the day, additional nitrogen oxide emissions (mainly from road traffic) in the modeled ozone curve led to a somewhat slower decrease compared to the dilution curve (cf. discussion on Fig. 18).

of magnitude within 24 hours. Such a behavior of the simulated ozone can solely be attributed to a lack of supply of background air in the model. Further detailed analysis by R.W. supports the fact that the lack of supply from ambient air in the simulation of VALM01 does also affect the simulations of NO_x and PM10.

The model evaluation group of the UC^2 project analyzed the causes of the deficits. Subsequently, the simulations were improved by the development group so that subsequent simulation were successful.

3.5.2 Analysis of the results of the simple PALM4U chemistry module (photostationary equilibrium) using VALM04 (Stuttgart, summer 2018).

The model results of the VALM04 validation run allowed a comparison of model results with the data from mobile observations for the first time. On two measurement days, 07/08/2018 and 07/09/2018, the Stuttgart valley basin and the upstream surrounding area were traversed several times by MobiLab. Figure 23b outlines the route of the Jülich mobile measurement laboratory.

For the modeling, a domain with 10 m resolution (Child 1 (N02)) and a domain with 2 m resolution (Child 2 (N03)) were fitted into the parent model domain with a resolution of 40 m (Figure 23a). The chemical and meteorological forcing data for PALM4U were obtained from the COSMO (**CO**nsortium for **S**mall-scale **MO**delling) model.

(a)

(b)
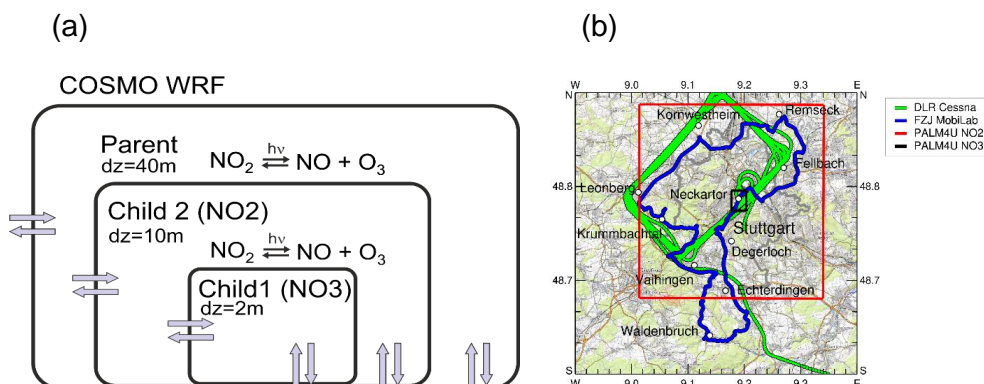
Figure 23 (a) Nesting of model domains of VALM04 modeling (07/08/2017 and 07/09/2017, Stuttgart, Germany) (Parent resolution: 40 m; Child 2 domain resolution (N02): 10 m; Child 1 domain resolution (N03): 2 m. The air chemistry module used in PALM4U consisted of the simple photochemical equilibrium approach without model realization of photochemical ozone formation.

(b) Spatial extent of the three model domains. Also, the travel and flight routes of the MobiLab (FZ Jülich) and the Cessna (DLR), respectively are shown on the right-hand site.

The comparison of the measured and simulated data shows that the spatial distribution of nitrogen oxides was well reproduced by the model. The relative decrease of nitrogen oxides (NO_x) north and south of Stuttgart corresponded to the observations (Figure 24). However, the increased concentrations on the A81 northwest of Stuttgart (see arrow in Figure 24) were not well reproduced by the model, possibly because the traffic assumed from density traffic flow model was too low. Traffic caused by long-distance-transport was underestimated by the local transport model.
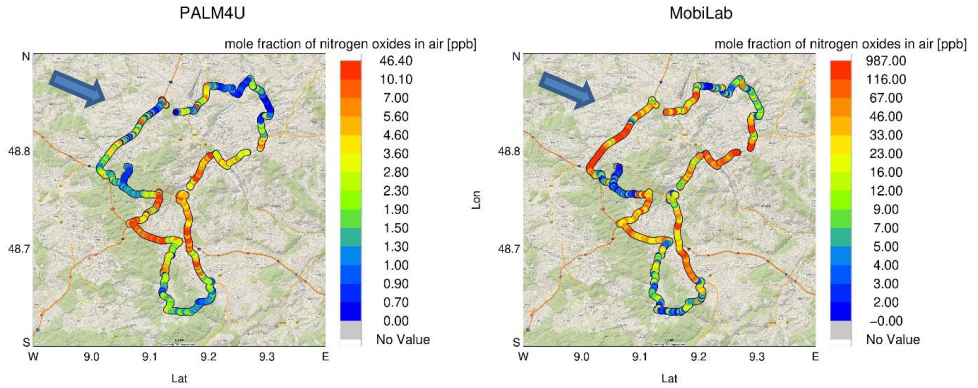
Figure 24 Simulated (PALM4U, left) and measured mixing ratios (MobiLab, right) of nitrogen oxides (NO$_x$) for 7/8/2018 (MobiLab measurement run from 10:57 - 14:04 (UTC)). The color code indicates the mixing ratios of the modeled and measured NO$_x$ values. The simulation shown is performed with the resolution of the parent domain as only the parent domain contained the complete MobiLab track.

The importance of spatial model resolution was proved by a detailed examination of the frequency distributions of both modeled and measured NO$_x$ (Figure 25). When comparing model and measured data from the parent domain, differences in the average NO$_x$ concentration of almost a factor of 7 were found (PALM4U[parent mean] : 7.6 ppb; MobiLab[mean] : 42.2 ppb). At 10 m resolution the difference was smaller, but the model still underestimates the measured values by a factor of 2.8.
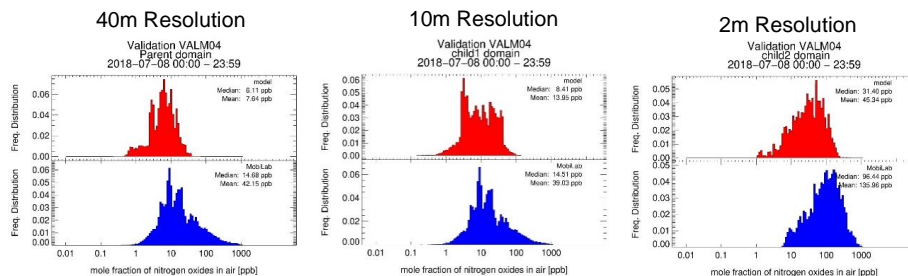
Figure 25 Frequency distributions of nitrogen oxides (NO_x) for simulated (PALM4U, top) and measured mixing ratios (MobiLab, bottom) of nitrogen oxides (NO_x) for 07/08/2018. Note that data from the child 1 domain and from the child 2 domain do not contain the complete dataset. Data of the child 2 domain were from the center of Stuttgart only.

The typical peaks observed in the highly resolved MobiLab dataset were also reproduced by the model (Figure 26). However, with the low model resolution the peaks were significantly lower than those of the NO_x MobiLab data. The improvement in agreement between model and measurement with improving resolution can be understood by the fact that not only the resolution in the horizontal but also in the vertical is improved from 40 m to 10 m. This means that the lowest grid box in the parent domain is on average 20 m above ground, while it is 5 m above ground for the child 1 domain. As the concentration of the pollutants is reduced with distance from the source, this artificial dilution in the large grid box of the parent domain will inevitably lead to an underestimation of the observed NO_x concentrations.

As the purpose of the measurements on 07/08/2018 was the study of the surroundings of Stuttgart, only a few measurements were done within the area of the child 2 domain with the highest model resolution of 2 m. A comparison is therefore only possible to a limited extent. Still, when using the output of the highest-resolved child 2 in the city center of Stuttgart, the model underestimated the observed NO_x by a factor of three.
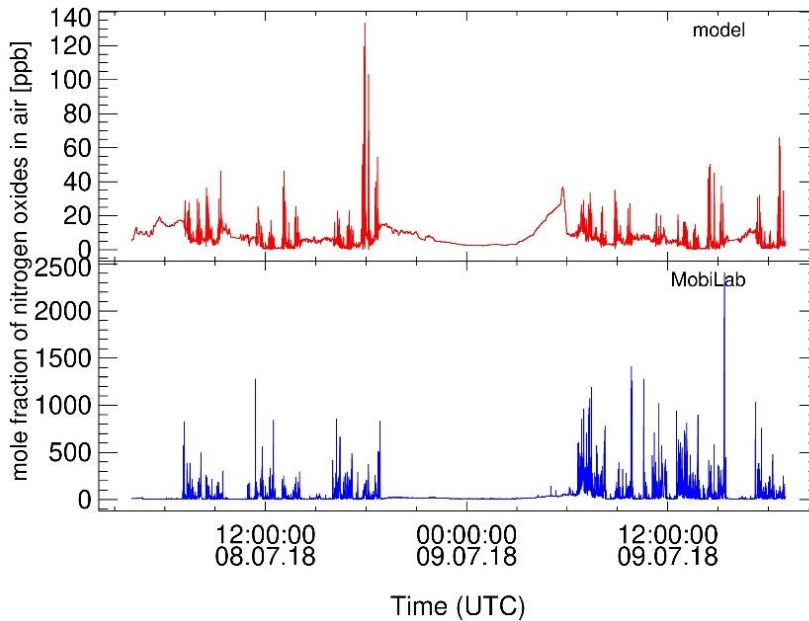
Figure 26 Time dependence of nitrogen oxides (NO_x) for simulated for the parent domain (PALM4U, top) and measured mixing ratios (MobiLab, bottom) for the intensive campaign VALM04, Stuttgart.

Since the typical travel distance of MobiLab at a speed of 20 km/h and the smallest time resolution of the MobiLab NO_x measurements of 2 s is about a factor of 5 larger the smallest spatial step size of PALM-4U, the underestimation of the NO_x in the model is attributable to the traffic emission module.

The validation of PALAM4U showed that:
- The PALM4U simulations reproduced the relative NO_x distribution as measured by MobiLab well.
- The agreement between the model and measured data improved with higher resolution.
- PALM4U underestimated the nitrogen oxide concentrations observed by MobiLab by a factor 2 – 3, even at the highest model resolution. The traffic emission module was identified as the likely source for this discrepancy.

3.5.3   Investigations on ozone production from the PALM4U chemical module CBM4: comparison of results with those of an explicit zero-dimensional model (MCM 3.3.1).

All model runs calculated within the second phase of the "Stadtklima" within the MOZAIC module were performed using simple mechanisms based solely on the "photostationary equilibrium" (equation 4). Under solar irradiation, NO_2 is photolyzed to NO (equation (1)). The resulting oxygen atom recombines with molecular oxygen O_2 to form ozone (equation (2)). The NO formed in equation (1) can react again with ozone (equation (3)) to form NO_2.

$$NO_2 + \text{hv} \longrightarrow NO + O(^3P) \qquad (1)$$

$$O(^3P) + O_2 + M \longrightarrow O_3 + M \qquad (2)$$

$$O_3 + NO \longrightarrow NO_2 + O_2 \qquad (3)$$
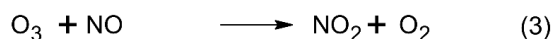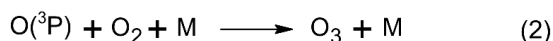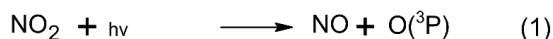
This is a rapid equilibrium that is shifted to NO and ozone under sunlight.

$$NO_2 \xrightleftharpoons{\text{hv}} NO + O_3 \qquad (4)$$
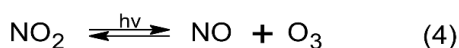
This chemistry model has the advantage of being very simple and requiring little computational time [Khan et al., 2021], because it contains only four variables and two reactions. However, the mechanism cannot describe photochemical ozone formation. This requires peroxy (RO_2) or hydroperoxyl radicals (HO_2) formed from volatile organic compounds (VOCs) and/or CO and which can produce NO_2 from NO with subsequent ozone formation, see reactions (5) and (6) where R stands for various hydrocarbons.

$$RH \xrightarrow[-H_2O]{+\dot{O}H} R^\bullet \xrightarrow{+O_2} RO_2^\bullet \qquad (5)$$

$$RO_2^\bullet + NO \longrightarrow NO_2 + RO^\bullet \qquad (6)$$
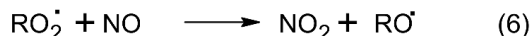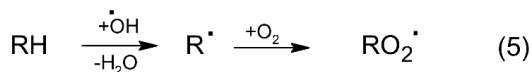
PALM4U can be operated with several more complex chemistry modules. The most elaborated is the CBM4 (Carbon Bond Mechanism) mechanism with 32 components and 81 reactions [Gery et al., 1989]. Even with this relatively simple mechanism, the relative computational time is roughly a factor of 15 larger compared to the simulation without the chemistry module [Forkel et al., 2018]. Therefore, all air chemistry simulations from the MOZAIK module were solely based on the photostationary equilibrium. However, ozone production can only be simulated with a more complex chemistry model such as the CBM4 mechanism.

3.5.3.1 *Comparison of local ozone production of CBM4 and MCM 3.3.1*

The hydrocarbons forming the peroxy radicals are diverse and originate from different sources such as traffic or vegetation. The simulation of the individual reaction steps is correspondingly complex and can in a computationally complex LES model like PALM4U only be done if individual components and reactions are summarized ("lumped"). However, lumping substances can lead to a significant deviation in the simulated ozone production. Therefore, prior to the PALM4U simulations (cf. chapter 0), the ozone production of the CBM4 mechanism was first compared to the Master Chemical Mechanism (MCM 3.3.1), an explicit chemistry model [Jenkin et al., 1997]. The MCM 3.3.1 mechanism is based on more than 5800 compounds and more than 17000 reactions. To test the models both models were run as 1-dimensional box models and the following model outcomes were compared:

- local ozone production
- ozone production in the course of one day (cumulative ozone production) when polluted airmasses are transported a from the city to rural areas

For both cases an average mix of hydrocarbons was used (cf. Figure 27), as it had been observed by us within the 3DO project in central Berlin. The general relationship between precursor concentrations of nitrogen oxides and hydrocarbons has already been illustrated using Figure 9, and reference has been made to the usefulness of reactivity considerations.

To perform the comparisons of local ozone production between the two mechanisms for a variety of precursor ratios, again the isopleth representation is used. In the next step, the initial VOC and NO_2 reactivity were varied; the ozone production after 10 minutes was simulated with MCM 3.3.1 and CBM4 respectively and visualized by means of an isopleth diagram (Figure 30).
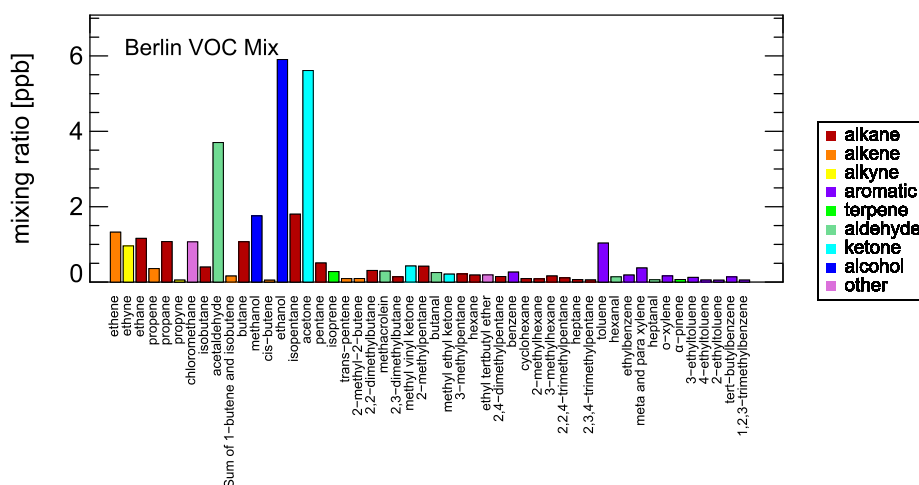
Figure 27 Mean measured mixing ratios of selected volatile organic compounds (VOC) from traffic (Berlin, summer 2017, mean value from 26 canister samples analyzed by GC/MS).

The following boundary conditions were used to compare local ozone production:

- Radiation conditions: clear-sky conditions, June 21st
- Temperature: 25° C
- Geographical position: 52.5° northern latitude

- Emission start: 12:00 local time
- Initialization time[14] of the model ("Parboiling" of the city mix): 600 s
- The same radiation parameters for both models
- Ozone background concentration: 50 ppb

For this model comparison[15], all input variables, meteorological boundary conditions and the integrator (FACSIMILE) [Curtis, 1980] were chosen to be the same for both models, so that any differences that occur can be clearly attributed to the photochemical calculation process or to the consequences of "lumping" in CBM4. A first insight into the differences of the photochemical processing is provided by a comparison of the OH concentration formed after the initialization time (Figure 8).

---

[14]The selected model initialization duration ("boil-on time") of 600 s ensures that photostationary equilibrium has been established within this time period for all selected start conditions.

[15] D. K. and U. J. thank D. Taraborelli (IEK-8, FZ Jülich) for valuable tips in converting the CBM4 model [Gery et al., 1989] into the FACSIMILE code.
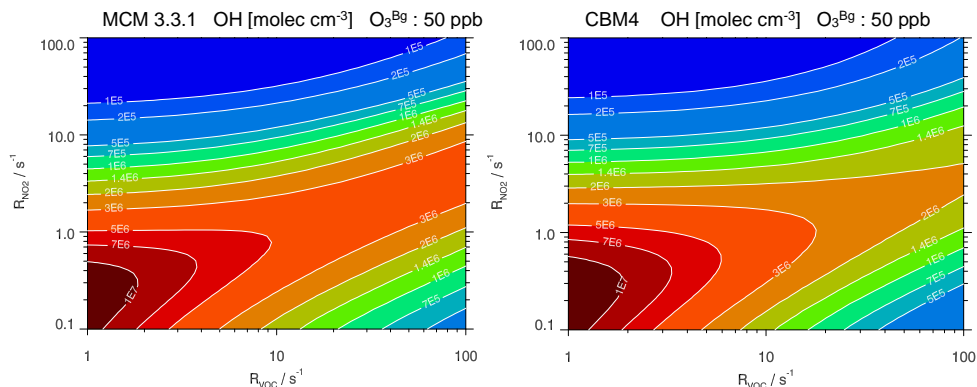
Figure 28 Local OH mixing ratio in molec. cm^{-3} as a function of VOC and NO$_2$ reactivity. The diagrams are based on the Master Chemical Mechanism MCM-3.3.1 (left) and the Carbon Bond Mechanism (CBM4, right), respectively. The same VOC mix was applied for both isopleth diagrams (see Figure 27). General conditions: Latitude: 52.5° north, radiation conditions: 06/21, local start time 12:00, calculation time period: 600 s, ozone background concentration (Bg): 50 ppb.

- Both models predicted highest OH concentrations (MCM and CBM4: > 1×10^7 molec. cm^{-3}) were at smallest R$_{VOC}$ and R$_{NO2}$ reactivities. With increasing R$_{NO2}$, steadily decreasing OH concentrations were found in both models.

- With increasing R$_{VOC}$, a "band" of elevated OH concentrations was apparent for both mechanisms in the region of optimal VOC/NO$_2$ ratios. The MCM mechanism yields approximately 30 % higher OH concentrations in this range for high R$_{VOC}$ reactivities.

- Overall, the isopleth plots for OH of both models were extraordinarily similar. Both the nitric oxide limitation of the MCM at low R$_{NO2}$ reactivities and the VOC limitation at high R$_{NO2}$ reactivities were almost perfectly reproduced by the CBM4 mechanism.

- The isopleth plots for OH of both mechanisms agreed within 30% for the diversity of the investigated (R$_{VOC}$, R$_{NO2}$) starting ratios. This proves the applicability of the "lumping" procedure used for CBM4. Unlike MCM, where explicit photochemical processing is performed for the individual VOCs (> 120 VOCs), there are only 11 substance classes needed in CBM4.

It has already been pointed out in chapter 3.5.3 that no additional ozone is produced from the photostationary equilibrium. Only if NO reacts with HO_2 or RO_2 radicals instead of ozone (cf. the explanations in chapter 3.5.3), a net ozone production ($P(O_3)$) occurs.

$$P(O_3) = [NO](k_1[HO_2] + k_2[RO_2]) \qquad (7)$$

Hence, the sum of HO_2 and RO_2 ($HO_2 + RO_2$) radicals indicates[16] the respective ozone production $P(O_3)$ at a given NO concentration (cf. Figure 29).

- For high R_{NO2}, the isopleth plots for both models show almost identical ($HO_2 + RO_2$) trajectories over the entire VOC range, suggesting similar ozone production rates for both mechanisms in this region of the $P(O_3)$-isopleth plot (Figure 30).

Figure 29 Sum of local ($HO_2 + RO_2$) concentration in molec./cm^3 as a function of R_{NO2} and R_{VOC} reactivity. The diagrams are based on the Master Chemical Mechanism MCM 3.3.1 (left) and the Carbon Bond Mechanism (CBM4, right), respectively. The same VOC mix was applied for both isopleth diagrams (see Fig. 27). General conditions: Latitude: 52.5° north, radiation conditions: 06/21; local time: 12:00.

---

[16] The NO concentration should not differ for both mechanisms, since in both cases it represents the result of the PSS at the same J_{NO2} and the same background ozone concentration.

- However, with decreasing R_{NO_2} below 1 s^{-1}, approximately 30% higher (HO$_2$ + RO$_2$) concentrations were found for the CBM4 mechanism at low R_{VOC} reactivities. This fact is reflected in higher ozone production rates for CBM4 (cf. Figure **30**30). An underestimation of the radical losses due to radical-radical reactions in the CBM4 mechanism can be primarily considered as an explanation for the deviations.

The behavior of the (HO$_2$ + RO$_2$) concentrations as a function of the R_{VOC} and R_{NO_2} starting ratios clearly defines the shape of the isopleth plots for P(O$_3$)[16]. The differences found in Figure 30 (30 % higher (HO$_2$ + RO$_2$) concentrations for CBM4 at small VOC reactivities and about 30 % higher (HO$_2$ + RO$_2$) concentrations for MCM 3.3.1 at highest VOC reactivities of 100 s^{-1}) are reflected in the P(O$_3$) isopleth plots. Here, the deviations of CBM4 compared to MCM at very high R_{VOC} are of only of rather academic interest, since this R_{VOC} reactivity range is well above typical European outdoor air conditions.
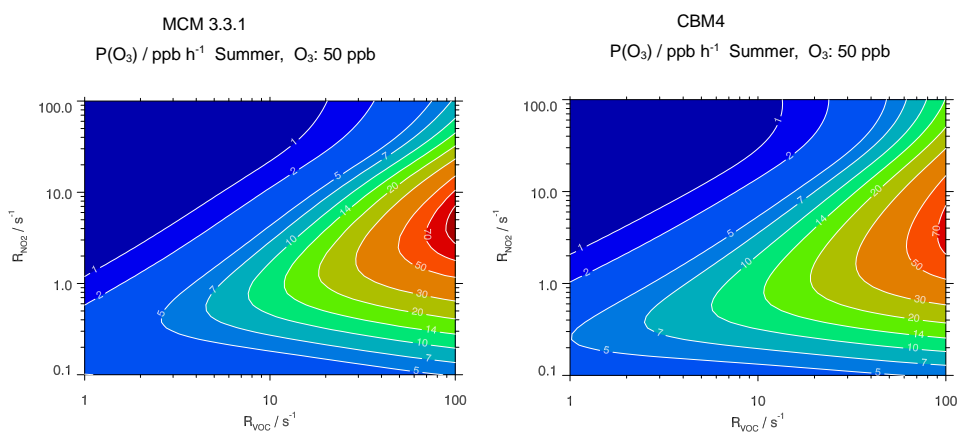
Figure 30 Local O$_3$ production rates [P(O$_3$)] in ppb h^{-1} as a function of VOC and NO$_2$ reactivity to OH radicals. The diagrams are based on FACSIMILE calculations with the Master Chemical Mechanism MCM 3.3.1 (left) and the Carbon Bond Mechanism (CBM4, right), respectively. The same VOC mix was applied for both isopleth diagrams (see Fig. 27). General conditions: Latitude: 52.5° north; radiation conditions: 06/21; local time 12:00.

Conclusions:

- Comparison of MCM 3.3.1 with the CBM4 mechanism proved the similarity for local ozone production rates $P(O_3)$ over a multitude of R_{VOC}, R_{NO2} input values in all ranges.

- In the range of relevant outdoor air VOC reactivities ($2\ s^{-1} < R_{VOC} < 10\ s^{-1}$), the CBM4 overestimates ozone production by about 30% compared to the MCM.

3.5.3.2 Comparison of ozone production over the course of a day (cumulative ozone production) when a polluted air mass is transported from urban to rural areas

A second comparison of the two "zero"-dimensional chemistry mechanisms (MCM-3.3.1 and CBM4) is based on the determination of the respective cumulative ozone production in an airmass on a given "transport path" from the source in the inner city into rural surroundings. In contrast to the studies on local ozone production in the previous chapter, the focus here is on the processing of urban emissions over the course of the day and on the increasing significance of the photochemical degradation products produced in the process over the course of the day. In detail, this comparison is based on the following scenario:

On the "transport path", this airmass experiences both photochemical degradation and dilution with unpolluted air masses. This initially leads to a decrease in the OH reactivity of both VOCs (R_{VOC}) and NO_2 (R_{NO2}). In biogenically dominated background environments, the OH reactivity of VOCs increases again due to compounds emitted by plants, while that of nitrogen oxides continues to decrease due to the dilution processes taking place. The ozone produced over the day[17], the so-called "cumulative ozone production" is compared for the two chemical mechanisms.

The boundary conditions of the model scenarios for the comparative evaluation of the ozone production of the two chemistry mechanisms were (Figure 31):

[17] The approach used here was originally developed by us for comparative assessment of different exhaust emission mixes [Polinowski et al., 2022]. Here, we use this approach to compare the results of cumulative ozone production for two different chemistry mechanisms.

- The starting reactivity[18] was set to $R_{NO2} = 17.6 \text{ s}^{-1}$ and $R_{VOC} = 10.1 \text{ s}^{-1}$. This corresponds to the summertime inner city average as observed in Berlin in 2017 - 2018 [Klemp et al., 2020]. The averaged VOC mix from the inner city of Berlin in 2017 (IOP-2) and 2018 (IOP-4) was used as input for the following studies. Its detailed composition is described in [Klemp et al., 2020].

- Near the biogenic source, in the background of the city, OH reactivity of VOC is considered[19] to be 7 s^{-1}.

- For the comparative evaluation of the two chemistry mechanisms, the measured (via cylinder samples by GC/MS) exhaust gas concentrations of hydrocarbons and oxygenated substances ($C_2 – C_{12}$) were used.

- For the temporal behavior of the composition of the VOC mix (see Figure 27), it was assumed for simplicity that anthropogenic NO_x, CO and VOC were released in the morning, diluted during subsequent transport into the surrounding biogenically dominated background areas, and photochemically processed. The increasing importance of biogenic VOC in the background area was reflected in its increasing fraction of the total VOC reactivity.

- Since there is no comparable biogenic source for nitrogen oxides, continuous dilution was assumed on their transport path from the city to the background areas.

- For the model comparisons of MCM-3.3.1 and CBM4, the following boundary conditions were chosen:
    o Berlin, 52° 30' N summer conditions.
    o Highest solar altitude (June 21st).
    o Equal temperature profile, and cloud-free conditions.
    o Start of the model runs 6:00.
    o 128 single steps with 300 s duration each, for each single step: reset of the starting conditions with modified initial values keeping the photochemical products generated in the model as additional VOC.

---

[18] It should be noted that the starting reactivity R_{NO2} in the model is established in a diurnal manner via photostationary equilibrium (PSS). The selected conditions ($O_3 = 50$ ppb, solar position for 06/21, coordinates for Berlin, NO= 66 ppb and, $NO_2 = 33$ ppb) result an R_{NO2} of 17.6 s^{-1} after the equilibrium setting of the PSS.

[19] The level of background biogenic VOC concentrations was adjusted to the reactivities measured during the ECHO campaign [Mittermaier & Klemp, 2004] and fed into the model as isoprene equivalents.

  - Deposition processes of the species involved were left out for this model comparison.

- In both cases the same concentration and temporal behavior for both biogenic VOCs and CO where assumed for the model runs. Their concentration change was taken into account in the models when updating the total reactivity towards OH ($R_{tot} = R_{VOC} + R_{CO}$). The same VOC mix was used for both model runs (MCM 3.3.1-daily cycle and CBM4-daily cycle).

- The model study spanned the NO$_2$ reactivity ranges of $0.1 \text{ s}^{-1} < R_{NO2} < 20 \text{ s}^{-1}$ and $1 \text{ s}^{-1} < R_{VOC} < 10 - 15 \text{ s}^{-1}$. Recent studies of Berlin and Stuttgart showed that the selected range of values represents the current typical dynamic range of summertime central European reactivities for NO$_2$ and VOCs in both polluted urban areas and background areas [Bonn et al., 2016; Klemp et al., 2021].

MCM 3.3.1
P(O$_3$) / ppb h^{-1} Summer, O$_3$: 50 ppb

Procedure:

- Start at the source (city center)
- Same starting conditions:
  R$_{VOC}$: 10.1 s^{-1}
  R$_{NO2}$: 17.6 s^{-1}
- Simulation of the dilution and processing of an air mass on the isopleth plot from 06:00 to 17:00
- Comparison of total ozone production rates as function of the time of the day
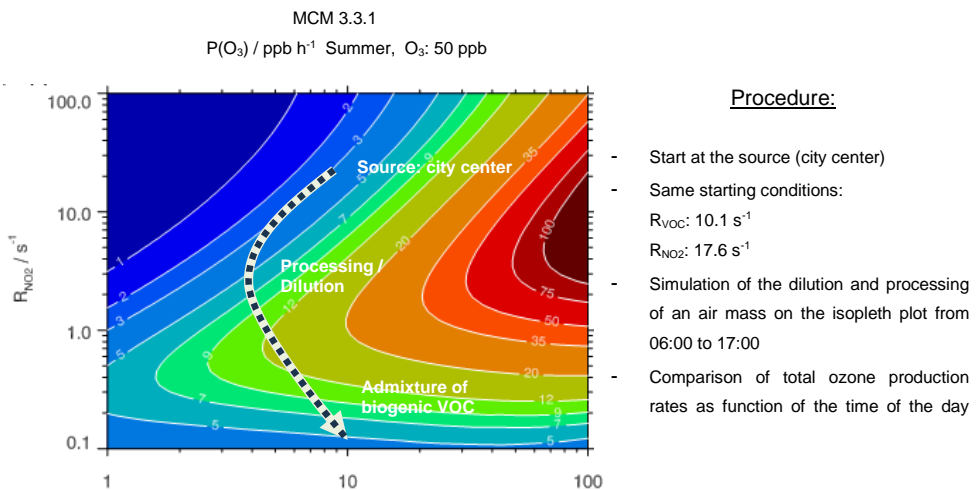
Figure 31 Isopleth plot of ozone production (P(O$_3$)) in ppb/h for 12:00 noon. The starting point at the "city center" reflects the average ambient conditions (R$_{NO2}$ = 17.6 s^{-1}, R$_{VOC}$ + R$_{CO}$ = 10.1 s^{-1}) as measured in Berlin 2017 (Summer, IOP-2 and Berlin, 2018, IOP-4). The curve represented describes the changes of R$_{VOC}$ and R$_{NO2}$ on the "transport path" of this airmass from the city center to the rural surroundings.

Figure 31 presents the procedure for the comparative P(O$_3$) assessment of MCM and CBM4 in context. It should be noted, however, that the isopleth plot depicted here only describes the situation at noon quantitatively. For all other times of the day, smaller

P(O$_3$) production rates than those shown here were applied during the processing and dilution pathway.

In Figure 32 is shown the time dependance of R_VOC_total + R_CO of the used VOC mix.
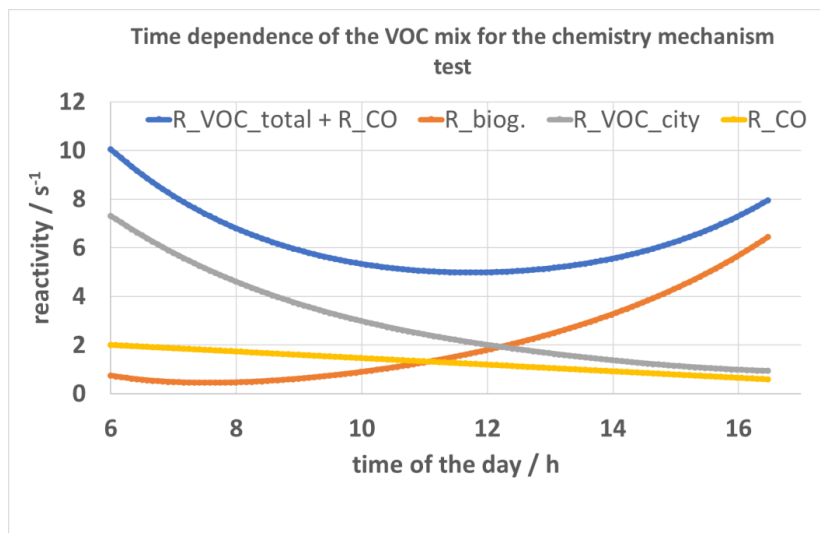
Figure 32 Time dependence of the VOC mix proportions to R_VOC_total + R_CO: An idealizing assumption is made that the VOC emission mix released in the morning originates from the "city" source alone and is continuously diluted on the transport path to rural areas. The same assumption was made for CO, starting at about 2 s^{-1} at the source and about 0.5 s^{-1} in background areas [Klemp et al., 2020]. Near the source, the biogenic fraction of the VOC mix (R_biog.) is initially low compared to the anthropogenic VOC fraction (R_VOC_city). It increases with increasing distance from the anthropogenic VOC source.

Figure 33 shows the ozone formation calculated for both MCM and CBM4 as a function of time of day. During the first 4 hours after release, the ozone formation rates of both

mechanisms hardly differed. Due to the ongoing dilution, the increasing photolysis rates and the additional input of biogenic VOCs, the ozone production rate $P(O_3)$ increased by almost one order of magnitude.
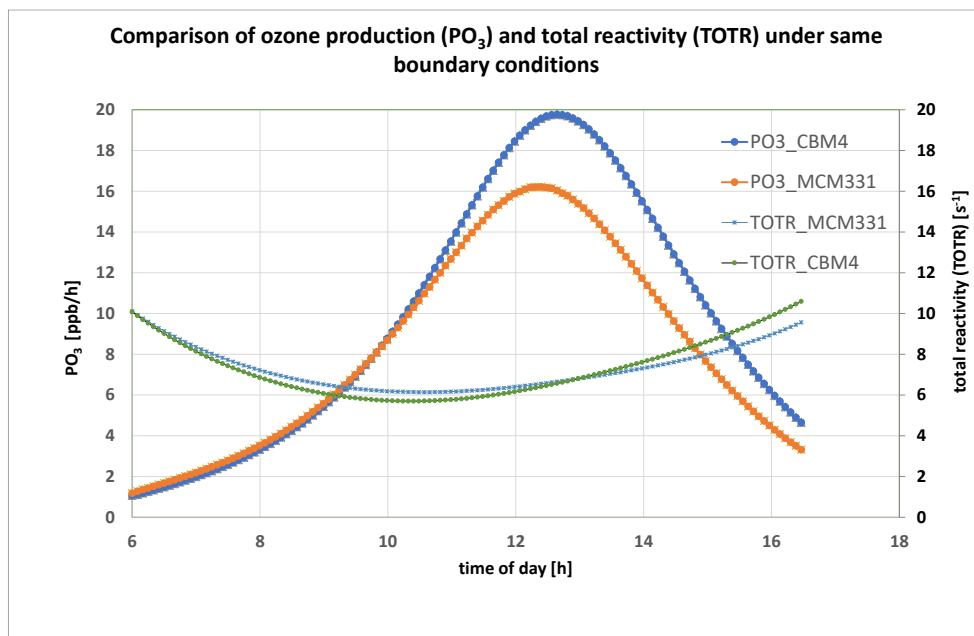
Figure 33 Ozone production ($P(O_3)$) in ppb/h and temporal evolution of the VOC reactivity as a function of time of day. The starting point at the "source city center" is emitted at 6:00 the averaged "Berlin city center mix" (average from: IOP-2 and IOP-4)) with the mean starting immission ratio ($R_{NO2} = 17.6$ s^{-1}, $R_{VOC} + R_{CO} = 10.1$ s^{-1}) measured by us. The same boundary conditions were chosen for both chemistry mechanisms.

At about the same time as the increase in biogenic VOCs, indicated by the increase in total reactivity after passing through the minimum in Figure 33, the ozone formation predicted by the CBM4 mechanism exceeded that from MCM 3.3.1 by more than 20%. At the same time, the total reactivity simulated by CBM4 (TOTR_CBM4) rose significantly faster than simulated by MCM 3.3.1, reaching a 10% higher reactivity value towards the end of the model period. It can be seen that most of the observed reactivity difference between CBM4 and MCM 3.3.1 resulted primarily from higher HCHO production caused by isoprene processing (Figure 34). Over the entire

simulation period, the average ozone production rate in CBM4 exceeded that in MCM 3.3.1 by 17 % (average ozone production rate MCM331: 8.36 ppb/h, CBM4: 9.8 ppb/h).
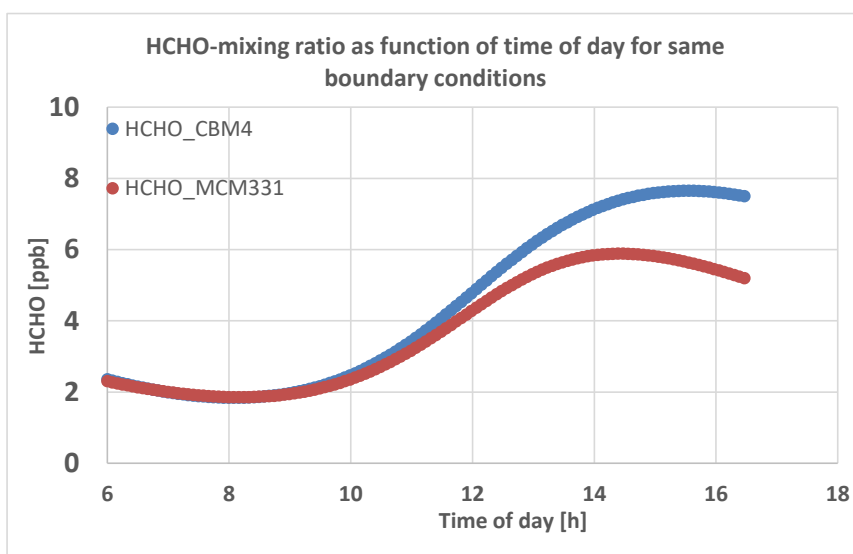
Figure 34 Temporal evolution of HCHO mixing ratio at the same starting value (2.5 ppb at the starting point "source downtown" at 6:00). The chemistry mechanism CBM4 produced up to 40% higher HCHO mixing ratios than MCM 3.3.1 as a result of the photochemical processing. The same boundary conditions were selected for both chemistry mechanisms.

The higher ozone formation after 10:00 a.m. compared to MCM is accompanied by an increased HCHO production from the processing of VOCs in CBM4 compared to MCM 3.3.1 (Figure 33 and Figure 34). HCHO promotes ozone production particularly efficiently [Nussbaumer et al., 2021], since this substance not only reacts with OH to form HO_2 radicals, but also produces two additional HO_2 radicals per HCHO molecule as a result of HCHO photolysis in one of the two photolysis channels. As this radical formation is independent of the NO_x level its importance rises at high NO_x conditions. The result can be seen in Figure 29. The CBM4 model yielded significantly higher (HO_2 + RO_2) concentrations than the MCM 3.3.1 mechanism at small nitrogen oxide

reactivities and in the range of moderate VOC reactivities, which is the actual cause of the increased ozone formation proposed by the model[20].

While processing, the CBM4 mechanism also led to an increased production of further secondary products, e.g. higher aldehydes, compared to the MCM mechanism. This is evident from the increased overall reactivity predicted by CBM4 compared to MCM. Here, only about 50% of the difference of about 1 s^{-1} at the end of the modeling period is caused by the enhanced HCHO formation of CBM4 (Figure 33)

Conclusions:

- The CBM4 mechanism predicted an about 20% increased ozone production compared to the reference MCM mechanism under background conditions and for moderate air chemistry loads.
- The reason for the increased ozone production was identified as the significantly increased aldehyde formation compared to MCM, with formaldehyde (approx. 2 ppb, corresponding to 0.5 s^{-1}) contributing the most.
- It is needed to extend such investigations to other VOC mixes for reliable photo-oxidant forecasts with PALM4U.

---

[20] A difference in NO concentrations in equation (7) cannot cause this effect, since the NO concentration in both mechanisms is controlled by the photostationary equilibrium.

3.6   Use of PALM4U in other applications

3.6.1   On the importance of the shadow effect on the NO/NO$_2$ ratio in a street canyon (PALM4U simulation using the simple PSS module).

The photolysis frequencies in the PALM4U chemistry model [Maronga et al., 2020] are calculated using the solar zenith angle-based parameterization from the Master Chemical Mechanism (MCM). The solar zenith angle for a given site is provided by PALM4U's internal radiation model. However, the MCM parameterization of photolysis frequencies is based on clear sky conditions, and it does not currently account for shadows cast by, for example, clouds or trees. Especially in an urban environment, large infrastructures cause shadows. Therefore, for accurate modeling, the influence of these obstacles on both photolysis frequencies and surface temperatures must be considered.

The surface temperatures in the PALM4U model are calculated using the radiation information from the implemented radiation model. However, the radiation model is not used to estimate the photolysis frequencies, but only to provide the solar zenith angle. This leads to an erroneous calculation of the concentrations of trace gases in shaded areas (e.g., street canyons). The influence of the shadowing effect on the concentrations was investigated by U. J. for a small area around Ernst-Reuter-Platz in Berlin with a sensitivity analysis.

Of particular interest was the model-based investigation of NO/NO$_2$ speciation in street canyons for different radiation conditions. From an air-hygienic point of view, the two nitrogen oxides (NO and NO$_2$) have to be evaluated differently due to their different health effects. While an immission limit value for the protection of health of 200 µg/m^3 (one-hour average) is set by law for NO$_2$, there is no comparable limit value for the trace gas NO. The high-resolution model PALM4U permits the meter-accurate simulation of NO/NO$_2$ speciation, which is particularly useful for urban areas with intensive building development (street canyons) close to roads.

The nitrogen oxides NO and NO_2 are in a rapid equilibrium[21] with ozone, which is governed by the photolysis of NO_2. Proper modeling requires accurate consideration of local shadowing at different zenith angles. This algorithm was not implemented at the time of our evaluations of the air chemistry module of PALM4U (as of 2021). To quantify the influence of the correct parameterization of shadow impact, model runs were performed with a modified version of PALM4U to evaluate the influence of the zenith angle of J_{NO2} on the NO/NO_2-ratio with and without shadow consideration in a street canyon the PALM4U simulation was set as follows:

- Model area : PALM4U Berlin, surroundings of the Ernst-Reuter-Platz, Intersection area of the east-west running Bismarckstraße with Leibnizstraße (Figure 35).
- Model domain: 960×960×1200 m, 10 m grid size
- Modelled time: 07/17/2017 00:00 – 24:00
- Boundary conditions used:
  - Photochemical mechanism: PSS.
  - "Clear-sky" conditions.
  - Cyclic boundary conditions.
  - Approximation of the shadow effect[22] depending on zenith angle and building shadowing, a building height of 25 m was considered[23].

---

[21] compare also the remarks on chapter 3. 5

[22] U. J. thanks R. Forkel (Atmospheric Environmental Research (IMK-IFU), Karlsruhe Institute of Technology (KIT)) and B. Khan (IMK-IFU, KIT) for providing the implementation of shadow approximations and related setup.

[23] Individual building heights for the parameterization of shadows are now available in the recent versions of PALM4U.

(a)   (b)
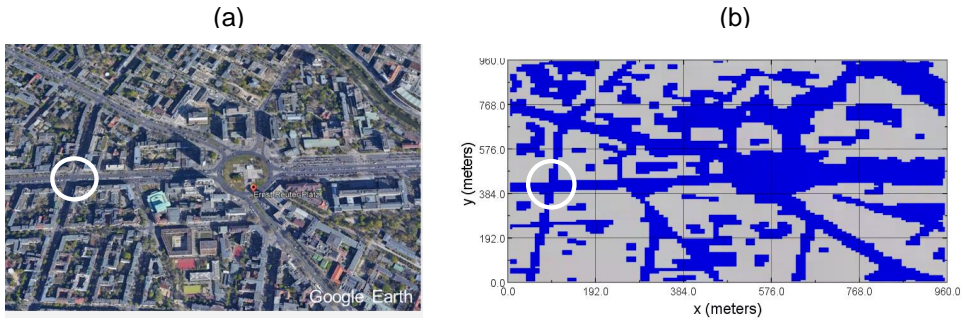
Figure 35 Model area Ernst-Reuter-Platz (Berlin) and considered street canyon intersection: (a) Google Earth representation; (b) implementation in PALM-4U.

Figure 36 shows an enlarged section of the model area for the intersection of Bismarckstraße running in east-west direction with Leibnizstraße in north-south direction. Three different simulation points were set up with increasing distances in north-south direction to the street mouth to Bismarckstraße. For these different points, which were 20 m apart the effect on shadowing of NO and NO_2 mixing ratios during the day were calculated. The diurnal course of the ratio ($NO^{shadow\ influence}$ / $NO^{without\ shadow\ influence}$) and ($NO_2^{shadow\ influence}$ / $NO_2^{without\ shadow\ influence}$) is shown in Figure 37.
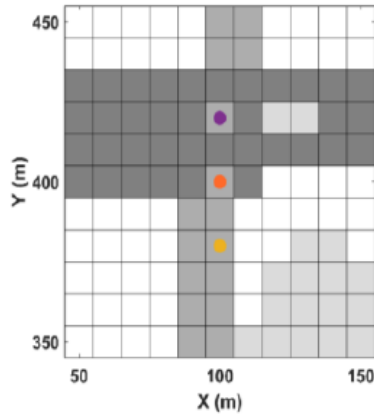
Figure 36 Intersection of Bismarckstraße (east-west course) and Leibnizstraße (north-south course). On both sides of Leibnizstraße there are 6 - 7-storey building rows (total height approx. 25 m each). Three different measuring points on the right side of Leibnizstraße (street width: approx. 20 m) are marked in color, each with an increasing distance of 20 m from the center of the intersection.
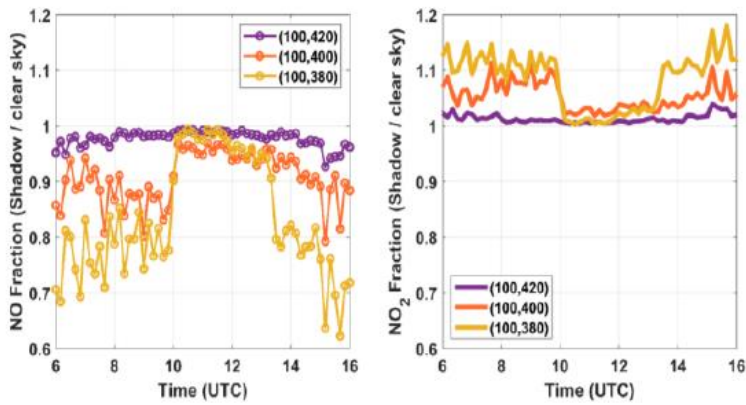
Figure 37 Diurnal course of the conditions ($NO_{shadow\ influence}$ / $NO_{without\ shadow\ influence}$) and ($NO_{2\ shadow\ influence}$ / $NO_{2\ without\ shadow\ influence}$) for three different measuring points on Leibnizstraße (road width: approx. 20 m) in the intersection area (violet) in the road junction (orange) and in Leibnizstraße (yellow). Color assignment and coordinates see Figure 36.

Various points were noted:

- With increasing distance from the intersection center, the influence of shadowing effects increased.
- The ratio (NO$_{shadow\ influence}$ / NO$_{without\ shadow\ influence}$) decreased by up to 30 %, since less NO is re-formed in the shade. This can be observed especially in the morning and evening hours, with a large zenith angle and corresponding shadowing.
- Depending on the prevailing NO/NO$_2$ ratio (which is either dominated by the exhaust emission ratio or approaches to the photostationary state at some distance from the source), the attenuated NO$_2$ photolysis in the shaded areas lead to an increase[24] of the NO$_2$ concentration by about 15 %.
- Shading effects lead to substantial increases in NO$_2$ concentration even at spatial scales of a few meters.

Conclusions:

- The strongest shadowing effects occur in narrow street canyons, and the peripheral areas of the streets with their pedestrian walkways located there are particularly affected.
- Neglecting the shadowing in street canyons leads to an overestimation of NO of up to 30 % and an underestimation of NO$_2$ of up to 15 %.

---

[24] In fact, the shadowing effects presented are also a function of the NO$_x$ concentration prevailing in the intersection area. In the model calculations presented here, the NO$_x$ concentrations at 5 m altitude were roughly about 10^0 - 10^2 ppb.

3.6.2 PALM4U simulation of the surroundings of Berlin's Ernst-Reuter-Platz using the PALM4U chemistry module with photochemical ozone production

The boundary conditions or constrains at the inflow of the PALM4U domain are important to drive a simulation under non-cyclic setups. For the meteorological components, the pathway for offline nesting based on the mesoscale weather prediction model COSMO-DE/D2 is well established (Figure 38). But there is a similar need to establish a robust pathway for the reliable offline nesting of chemical species[25]. Within this work we will demonstrate the successful linkage of the chemical transport model EURAD-IM (EURopean Air pollution Dispersion – Inverse Model) [Elbern et al., 2007], to PALM4U.

3.6.2.1 *First linkage of PALM4U to a current regional chemistry and transport model (EURAD-IM) for the relevant chemical components*

The use of the regional chemical transport model (CTM) EURAD-IM is particularly suitable for us as a supplier of the forcing of the relevant chemical components for PALM4U:

-   Daily regional model calculations in the Central European region are available for the period of several years, which can be directly used as chemical forcing data.
-   The EURAD-IM model system increases the quality of the model results by additional assimilation of results from fixed measuring stations.
-   The developers and operators of EURAD-IM are in our institute and can be consulted at any time if problems arise.

---

[25] A regular transfer of the chemical and meteorological data from a regional model to PALM4U is mandatory for the case of non-cyclical boundary conditions (as they are required for the adequate realization of a diurnal cycle), because only in this way diurnally varying quantities for chemistry and meteorology can be introduced into the PALM4U model.

- Any necessary adaptations and extensions of this CTM can be done in-house. These adaptations will most likely be required when operating a more sophisticated chemical module for PALM4U with photochemical ozone production.

(Kadasch et al., 2021)
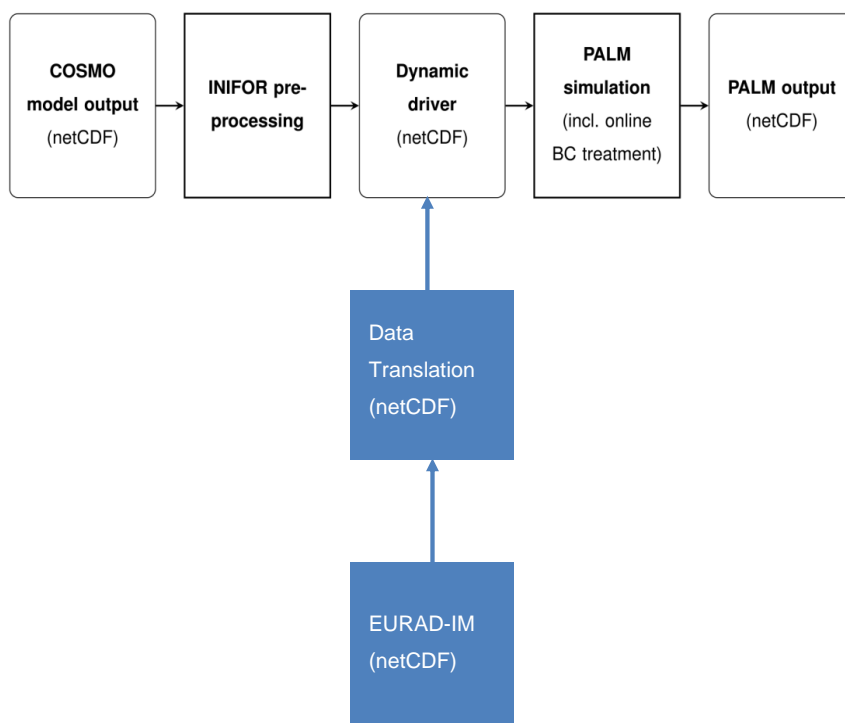
Figure 38 Existing transfer path for the meteorological components [Kadasch et al., 2021] as the input for PALM-4U and the new transfer path implemented by us (U. J.) (marked in color) [Javed et al., publication in preparation, 2024] for the output of EURAD-IM runs [Elbern et al., 2007]. In general, suitable forcing data of the meteorological and chemical components from a regional model are required for all 5 boundary areas of each PALM-4U model region (Figure 39). The figure shows the transfer of the "layer" distribution of the ozone field from EURAD-IM to the northern boundary of the PALM-4U model region.
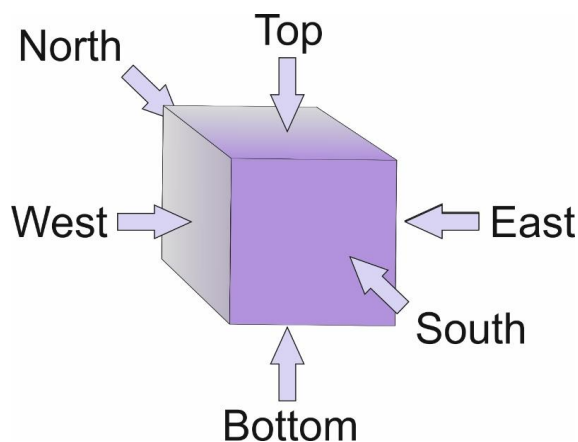
Figure 39 Schematic representation of the driving data of the meteorological and chemical components entered externally via the 5 boundary surfaces (North, South, West, East & Top) of the PALM4U model "cube" by EURAD-IM (chemistry) and COSMO-DE (meteorology).

In addition, at the beginning of the model run, PALM4U requires the definition of initial start conditions for chemistry and meteorology and the implementation of appropriate surface emissions of relevant chemical components within PALM4U.

It should be noted that, depending on the prevailing wind direction at any given time, the PALM4U model "cube" will be flushed and trace gas concentrations transported upwind by EURAD-IM will be transferred to the PALM4U "cube". This framework requires the PALM4U model to operate under non-cyclic boundary conditions (i.e., trace gas concentrations advected with wind flow and transferred to the PALM4U model region must be continuously updated by the results of a regional model).

Figure 38 shows the previously existing transfer path for the meteorological components [Kadasch et al., 2020] and our newly developed transfer path[26] for implementing the outcome of EURAD-IM into PALM4U.

---

[26] U. J. thanks E. Friese (FZJ, Jülich) for providing the EURAD-IM data along with an introduction to the infrastructure of EURAD-IM.

An example of successful linkage of chemical parameters calculated by EURAD-IM, the handover of ozone concentration varying in height and time of day at the northern boundary surface of the PALM4U model is shown in Figure 40 (i.e., the averaged regional wind vector is assumed to be perpendicular to the northern boundary surface of the PALM4U model "cube", see explanations for Figure 39.
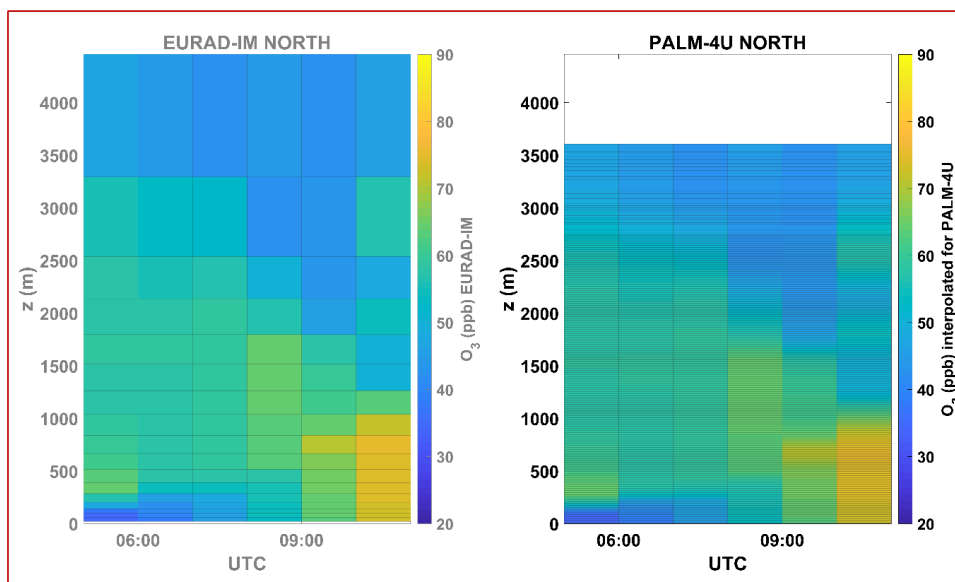
Figure 40 Result of the transfer of the ozone concentration varying in height and time of day from EURAD-IM shown at the northern boundary surface of the PALM4U model. The number of "layers" strongly deviated between EURAD-IM and PALM4U.

The height-time profiles of the hourly ozone concentrations calculated by EURAD-IM for the northern boundary surface were compared with the values transported into PALM4U. In particular, the strongly different number of "layers" between EURAD-IM and PALM4U (EURAD-IM about 20 up to a height of about 4000 m, PALM4U: several hundreds of "layers" at a distance of typically 10 m) required extensive interpolation calculations. Indeed, the result of these EURAD-IM interpolations provided a

concentration profile of PALM4U ozone values that was virtually identical in altitude and time, with the transitions between layers smoothed.

3.6.2.2 *Visualization of high-resolution calculations of oxidant formation for the surroundings of Ernst-Reuter-Platz in Berlin with PALM4U and the chemistry module CBM4*

Another goal of our investigations was the application of the PALM4U model package: The focus was on investigations of the dispersion of pollutants in street canyons as well as the first-time application and testing of chemical mechanisms with photochemical ozone formation within the PALM4U program package. For this purpose, we submitted a research proposal to the Jülich Supercomputing Center for computing time on the Jülich supercomputers.

The proposal was granted, so that we subsequently had sufficient computer resources to run PALM4U for Berlin with parent and child regions with good resolution. Subsequent simulations on the supercomputer were performed by U. J. after initial bugs related to PALM4U/supercomputer setups had been successfully removed[27].
The offline nesting into the EURAD-IM model [Elbern et al., 2007] was used to constrain the chemical as well as the meteorological parameters at the lateral and top boundaries of the PALM model domain. In each case, the EURAD-IM model provided the distribution of inorganic trace gases at the model boundaries[28]. The VOC data were linked to the NO_x emissions from the traffic model for Berlin using the measured VOC/NO_x ratios.

---

[27] U. J. gratefully acknowledge the support/time provided by the PALM group (Institute of Meteorology and Climatology (IMUC) of Leibnitz University Hannover) by the PALM4U setup and Olaf Stein (Institute for Advanced Simulation, JSC, FZ-Jülich for the supercomputing.

[28] We have also successfully tested to transfer of the necessary meteorological boundary parameters from EURAD-IM to PALM4U (instead of reading them from COSMO via the method developed by [Kadasch et al., 2021]). This reduces considerably the effort required to provide the necessary parameters from different regional models.

The simulation was performed for June 26th 2019 for an area[29] of 6.72x6.72 km with a spatial resolution of 10 m. Figure 41 shows the distribution of nitrogen oxides at 11:00 CEST. The concentration of nitrogen oxides depends not only on the traffic density but also on the built-up area, which hinders the removal of nitrogen oxides. Therefore, the highest nitrogen oxide values were not predicted for the urban highway, which runs in a north-south direction in the west of the model area, but for the densely built-up main roads in the center of the model area. The lower nitrogen oxide concentration on the part of Straße des 17. Juni[30] that runs through the Tiergarten in the east of the model area is obvious. The reason for the lower nitrogen oxide concentration compared to the inner city streets is the absence of buildings which hinders the ventilation in other parts of the city.

---

[29] The topography data is taken from [Khan et al. 2021] and further modified for our applications.

[30] Street crossing (Fig 41) in the center of the picture in a west-east direction with the Tiergarten in the eastern part of the picture.
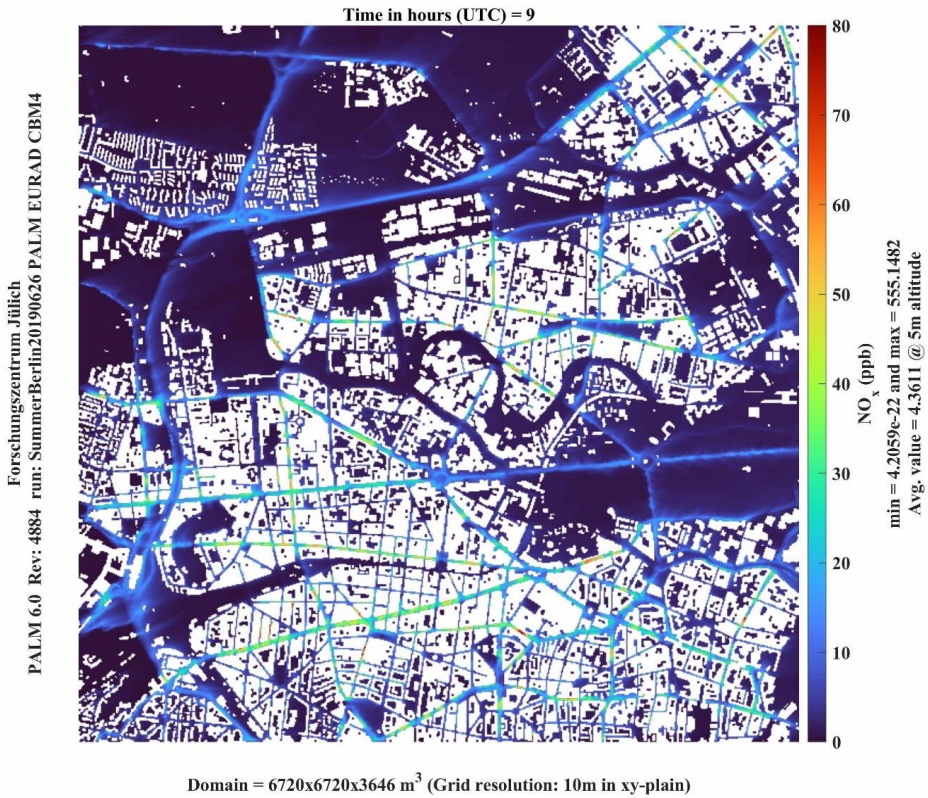
Figure 41 Horizontal NO$_x$ distribution at a height of 5m simulated with PALM4U and CBM4 mechanism for 6/26/2019 09:00 UTC. Wind from the west.

The ozone concentration (Figure 42) was strongly determined by background values transported from the outside into the city Berlin as predicted by the EURAD-IM model. Only in street canyons where strong traffic emissions of nitrogen oxides reduced its concentration, the ozone values were significantly lower than the respective values in the background.

The concentration of the radicals[31] RO_2 and HO_2 is determined on the one hand by the processing of the VOCs (reaction 5), and on the other hand by the reaction with NO (reaction 6). Here PALM4U showed its special advantages for short-lived radicals with its high temporal and spatial resolution: The spatial distribution of radicals routed over the roads and highways in the model area showed minima leeward of the magistrals (Figure 43). Further downwind, however, rapid photochemistry led to increases in radical concentrations where nitrogen oxide concentrations were low. The highest
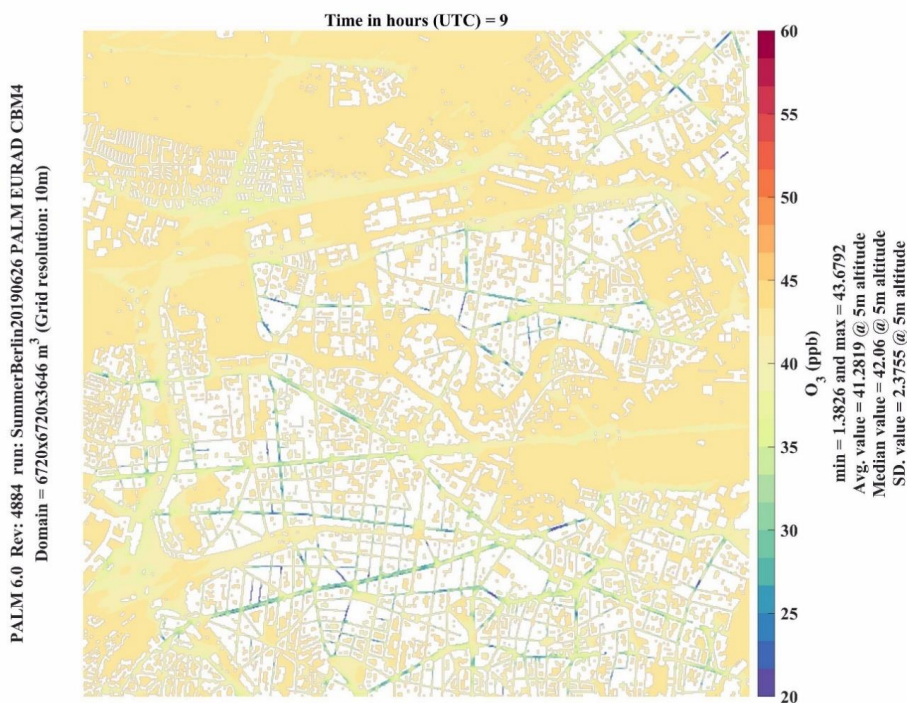
Figure 42 Horizontal ozone distribution at a height of 5m simulated with PALM-4U and CBM4 mechanism for 6/26/2019 09:00 UTC. Wind from the west.

concentrations were predicted immediately upwind of the magistrals before the concentrations decrease again due to the high NO concentrations at the roads. It is remarkable how clearly relatively small areas with lower traffic density in the northwest

---

[31] The sum of both radicals is named RO_x in the following.

of the model area with their elevated RO_x concentrations (cf. in the southwestern model sector (U-Bahn-Westkreuz, Halensee and Volkspark Jungfernheide) differed from other areas. In the densely built-up and congested urban area of Berlin Mitte, on the other hand, significantly lower RO_x concentrations were expected from the model.
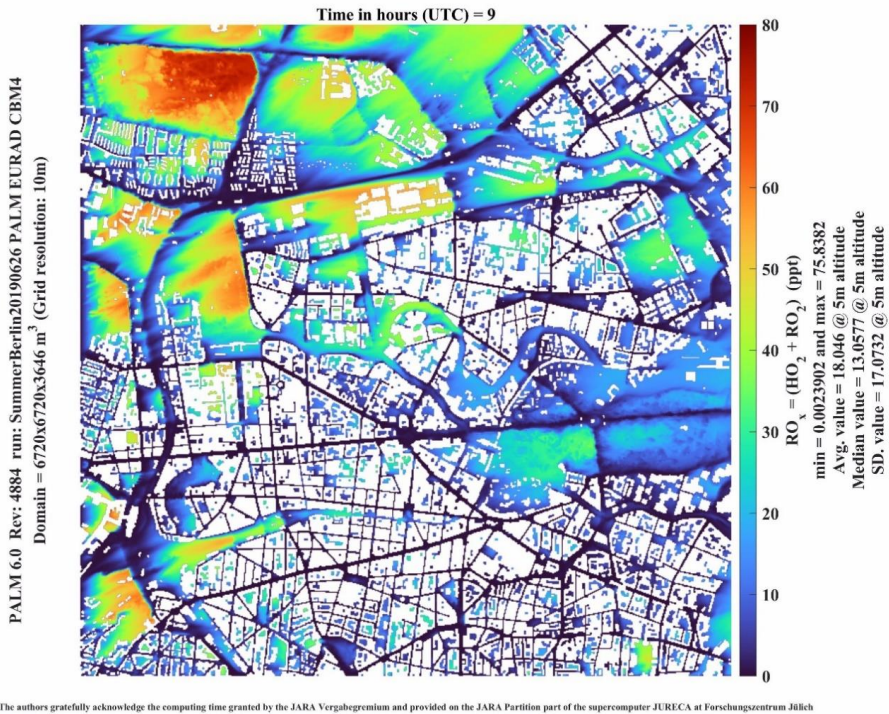
Figure 43 Horizontal distribution of RO_x at a height of 5m simulated with PALM-4U and CBM4 mechanism for 26.6.2019 09:00 UTC. Wind from the west.

Ozone production according to reaction (7) occurs only when hydroperoxyl and peroxy radicals react with NO (in contrast to reaction (4) from photostationary equilibrium, where the sum of $O_x = NO_2 + O_3$ remains constant).

Figure 44 shows that the turnover of radicals, and thus ozone production, was highest above the urban highway in the western part of the model area and in the Tiergarten

area in the eastern part. On the main roads in east-west direction, above which the nitrogen oxide concentration is highest, the ozone production was rather low. This
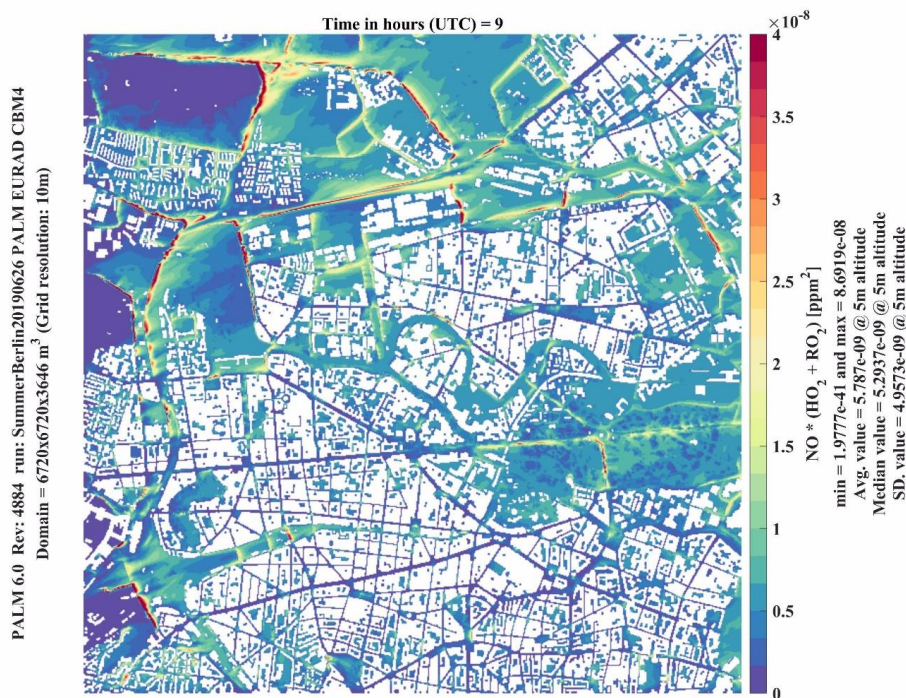
Figure 44 Horizontal distribution of P(O₃) according to reaction (7) at a height of 5 m simulated with PALM4U and CBM4 mechanism for 06/26/2019 09:00 UTC. Wind from the west.

shows that a built-up of RO_x over area with small NO_x concentrations is necessary for efficient ozone production.

The mean height profile demonstrates that ozone production occured predominantly near the ground (Figure 45). This is remarkable since analogous reactions also lead to the formation of other pollutants such as particulate matter. In addition, the simulation shows that the formation of secondary pollutants occurs not only on roads but also in the lee areas of roads. The results of the study emphasize the influence of traffic emissions on atmospheric chemistry in areas downwind of the emissions. Moreover, the observable intensifications of ozone production due to the interplay of

anthropogenic (road traffic) emissions and biogenic VOC emissions are remarkable (cf. e. g.: areas of the Tiergarten in the west of the model region).
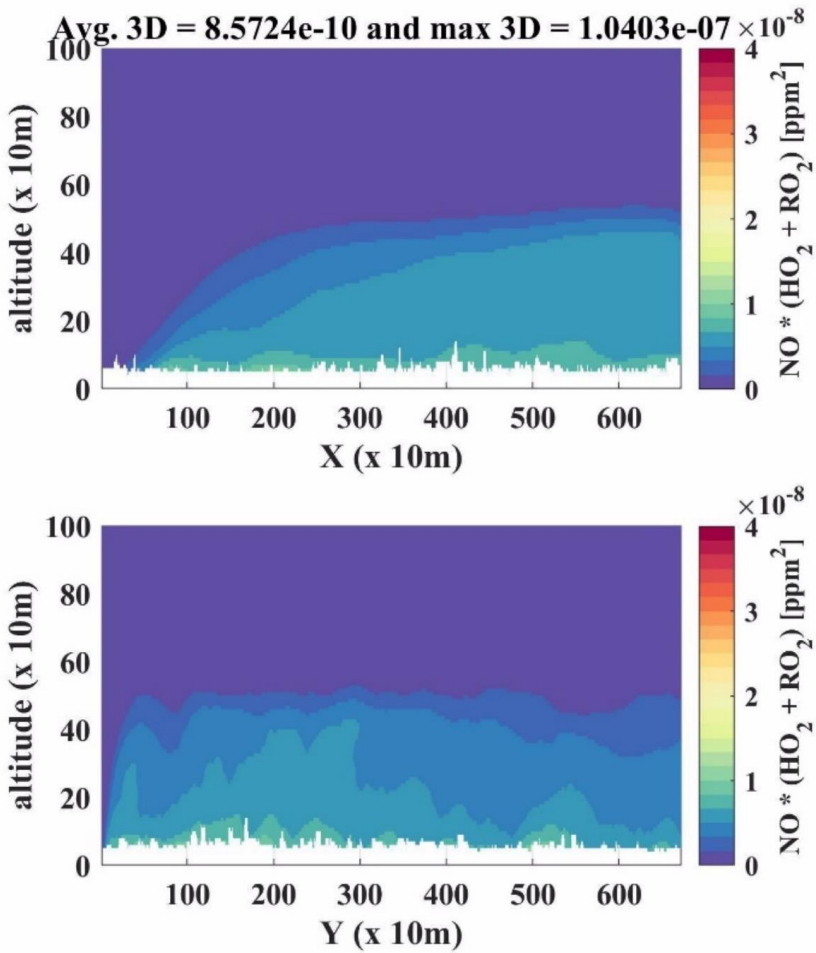
Figure 45 Vertical distributions of P(O₃) through the model region according to equation (7) looking west to and looking south to north simulated with PALM-4U using the CBM4 mechanism for 6/26/2019 09:00 UTC. Wind from the west.

3.7   Further applications of the results

The goal of the second phase of the funding measure "Stadtklima im Wandel" was the further development of the urban climate model PALM4U into a product suitable for practical use, which is oriented towards the needs of municipalities and other users. In the TP6 of module B, for which we were responsible, contributions were to be made to the evaluation of the urban climate model, and modules A and C were to be supported by special measurements. In addition, our work served to obtain input data for the model, to improve the chemistry module, and to evaluate the model as such.

The evaluation of the air chemistry module (photostationary equilibrium) of PALM4U was performed by us in the second part of the grant period. Weaknesses found were identified and eliminated in collaboration with Module A.

The success of the optimization procedures could be demonstrated by VALM04 evaluations.

In our own model studies with PALM4U, we successfully applied the air chemistry module CBM4 for the first time to obtain a differentiated picture of local summertime ozone formation for the inner city area of Berlin. For this purpose, in an independent development from the regional chemistry and transport model EURAD-IM, the forcing data of the relevant chemical components were transferred to PALM4U. This allows detailed studies with high spatial resolution using PALM4U to describe the effect of biogenic emissions (parks, different tree cover) on local photooxidant formation.

In one study, the photooxidant formation properties of CBM4 were compared with those of an explicit zero-dimensional model (MCM 3.3.1) and causes for the differences and causes were identified.

The data sets on the emission behavior of the current vehicle fleet that we generated in the second funding period are currently being used by the TU Berlin in the Institute of Transportation System Planning and Traffic Telematics to optimize the traffic emission module developed there.

At the end of the project, the data generated will be made available to universities and research institutions as well as, in the context of collaborations, to interested companies in accordance with the Helmholtz Association's open access policy (https://os.helmholtz.de/open-access/), while preserving all rights of the project participants.

The data set generated in this project is of considerable relevance beyond the actual project objectives:

Near-source trace gas measurements in tunnels reflect the emission conditions of the current vehicle fleet. When normalized to the CO_2 increase in the tunnel measured simultaneously with high time resolution, the quality of existing road traffic emission models can be experimentally verified. Since 2016, we have probed the Heslacher Tunnel annually with MobiLab over the duration of the project, so that a time series of the emission behavior of the respective current vehicle fleet is now available for more than half a decade[32]. The working group plans to continue these investigations as far as financial resources allow.

In the second phase of the funding period, a large number of canister samples were taken from various areas of the city of Stuttgart, in addition to numerous VOC samplings in the Heslacher Tunnel. Currently, as part of an ongoing dissertation, this data set is being used to determine the polluter contributions using Chemical Mass Balance. First results have already been presented [Karadurmus et al., 2022].

In addition, the current emission datasets obtained here can be used for extensive chemistry and transport modeling, so that robust statements on the atmospheric residence time of the introduced trace substances can also be derived.

Extensive measurements of atmospheric NH_3 concentrations were performed as part of the urban climate project. The emission ratio of NH_3/CO_2 in the exhaust gas of motor vehicles could be determined to a value of about 0.05 [ppb/ppm] based on tunnel studies. During the project period, we observed an increase in NH_3/CO_2 emission ratios of more than a factor of 3, which is mainly due to the introduction of SCR cats in diesel vehicles. We will use future long-term studies to quantify this newly occurring input of NH_3 from SCR-cat vehicles and investigate its significance for secondary particulate formation.

---

[32] Currently, these data sets are used in comparative modeling studies to evaluate the emission behavior of alternative fuels [Polinowski, 2023].

It is planned to make the temporally and spatially highly resolved data sets collected within the urban climate project also available for the assessment of traffic related health effects[33].

---

[33] Contacts already exist within the framework of a joint HGF project "SMARAGD" with the Helmholtz Centre for Infection Research.

4 Literature

Belusic, D., Lenschow, D. H., & Tapper, N. J. (2014). Performance of a mobile car platform for mean wind and turbulence measurements. Atmospheric Measurement Techniques, 7(6), 1825-1837. https://doi.org/10.5194/amt-7-1825-2014

Bonn, B., von Schneidemesser, E., Andrich, D., Quedenau, J., Gerwig, H., Ludecke, A., Kura, J., Pietsch, A., Ehlers, C., Klemp, D., Kofahl, C., Nothard, R., Kerschbaumer, A., Junkermann, W., Grote, R., Pohl, T., Weber, K., Lode, B., Schonberger, P., . . . Lawrence, M. G. (2016). BAERLIN2014-the influence of land surface types on and the horizontal heterogeneity of air pollutant levels in Berlin [Article]. Atmospheric Chemistry and Physics, 16(12), 7785-7811. https://doi.org/10.5194/acp-16-7785-2016

Brauers, T., & Hofzumahaus, A. (1992). Latitudinal variation of measured NO2 photolysis frequencies over the Atlantic Ocean between 50° N and 30° S. Journal of Atmospheric Chemistry, 15(3), 269-282. https://doi.org/10.1007/BF00115398

Coggon, M. M., McDonald, B. C., Vlasenko, A., Veres, P. R., Bernard, F., Koss, A. R., Yuan, B., Gilman, J. B., Peischl, J., Aikin, K. C., DuRant, J., Warneke, C., Li, S. M., & de Gouw, J. A. (2018). Diurnal Variability and Emission Pattern of Decamethylcyclopentasiloxane (D-5) from the Application of Personal Care Products in Two North American Cities [Article]. Environmental Science & Technology, 52(10), 5610-5618. https://doi.org/10.1021/acs.est.8b00506

Curtis, A. R. (1980). The FACSIMILE numerical integrator for stiff initial value problems Conference on computational techniques for ordinary differential equations, Manchester.

Ehlers, C. (2014). Mobile Messungen - Messung und Bewertung von Verkehrsemissionen, phD thesis, University of Cologne. Jülich. https://juser.fz-juelich.de/record/171858/files/FZJ-2014-05414.pdf

Ehlers, C., Klemp, D., Kofahl, C., Fröhlich, H., & Möllmann-Coers, M. (2016a). Untersuchungen zur Luftqualität in Bad Homburg (Vol. 353). Forschungszentrum Jülich GmbH. https://juser.fz-juelich.de/record/828291/files/Energie_Umwelt_353.pdf

Ehlers, C., Klemp, D., Rohrer, F., Mihelcic, D., Wegener, R., Kiendler-Scharr, A., & Wahner, A. (2016b). Twenty years of ambient observations of nitrogen oxides and specified hydrocarbons in air masses dominated by traffic emissions in Germany. Faraday Discussions, 189, 407-437. https://doi.org/10.1039/c5fd00180c

Elbern, H., Strunk, A., Schmidt, H., & Talagrand, O. (2007). Emission rate and chemical state estimation by 4-dimensional variational inversion. Atmos. Chem. Phys., 7(14), 3749-3769. https://doi.org/10.5194/acp-7-3749-2007

Forkel, R., Khan, B., Banzhaf, S., Russo, E., Kanani-Sühring, F., Ketelsen, K., Kurppa, M., & Maronga, B. (2018). Test of gas phase chemistry mechanisms for a LES model with online coupled chemistry. https://meetingorganizer.copernicus.org/EGU2018/posters/9595

Gery, M. W., Whitten, G. Z., Killus, J. P., & Dodge, M. C. (1989). A photochemical kinetics mechanism for urban and regional scale computer modeling [https://doi.org/10.1029/JD094iD10p12925]. Journal of Geophysical Research: Atmospheres, 94(D10), 12925-12956. https://doi.org/https://doi.org/10.1029/JD094iD10p12925

Jenkin, M. E., Saunders, S. M., & Pilling, M. J. (1997). The tropospheric degradation of volatile organic compounds: A protocol for mechanism development. Atmospheric Environment 31 (1997) 81-104.

Kadasch, E., Sühring, M., Gronemeier, T., & Raasch, S. (2020). Mesoscale nesting interface of the PALM model system 6.0. Geosci. Model Dev. Discuss., 2020, 1-48. https://doi.org/10.5194/gmd-2020-285

Karadurmus, L., Klemp, D., Wegener, R., Dubus, R., & Wahner, A. (2022). Elevated concentrations of ethanol in the tunnel and city center of Stuttgart. 9th Georgian-German School and Workshop in Basic Science (GGSWBS), Kutaisi and Tbilisi, Georgia.

Khan, B., Banzhaf, S., Chan, E. C., Forkel, R., Kanani-Sühring, F., Ketelsen, K., Kurppa, M., Maronga, B., Mauder, M., Raasch, S., Russo, E., Schaap, M., & Sühring, M. (2021). Development of an atmospheric chemistry model coupled to the PALM model system 6.0: implementation and first applications. Geosci. Model Dev., 14(2), 1171-1193. https://doi.org/10.5194/gmd-14-1171-2021

Klemp, D., Mannschreck, K., Pätz, H.-W., Habram, M., Matuska, P., Slemr, F. (2002). Determination of anthropogenic emission ratios in the Augsburg area from concentration ratios: results from long-term measurements. In Atmospheric Environment (Vol. 36, pp. S61-S80).

Klemp, D., Mihelcic, D., & Mittermaier, B. (2012). Messung und Bewertung von Verkehrsemissionen (Vol. 21). Forschungszentrum Jülich, Zentralbibliothek. https://juser.fz-juelich.de/record/22982/files/Energie%26Umwelt_21.pdf

Klemp, D., Wegener, R., Dubus, R., & Javed, U. (2020). Acquisition of temporally and spatially highly resolved data sets of relevant trace substances for model development and model evaluation purposes using a mobile measuring laboratory (Vol. 497). Forschungszentrum Jülich GmbH Zentralbibliothek, Verlag. https://juser.fz-juelich.de/record/878037/files/Energie_Umwelt_497.pdf

Klemp, D., Wegener, R., Dubus, R., Karadurmus, L., Kille, N., & Tan, Z. (2021). Distribution of trace gases with adverse effects on fuel cells (Vol. 539). Forschungszentrum Jülich GmbH Zentralbibliothek, Verlag.

Maronga, B., Banzhaf, S., Burmeister, C., Esch, T., Forkel, R., Fröhlich, D., Fuka, V., Gehrke, K. F., Geletič, J., Giersch, S., Gronemeier, T., Groß, G., Heldens, W., Hellsten, A., Hoffmann, F., Inagaki, A., Kadasch, E., Kanani-Sühring, F., Ketelsen, K., . . . Raasch, S. (2020). Overview of the PALM model system 6.0. Geosci. Model Dev., 13(3), 1335-1372. https://doi.org/10.5194/gmd-13-1335-2020

Mittermaier, B., & Klemp, D. (2004). Speciated Analysis of biogenic VOCs during the ECHO-Campaign. EGU General Assembly 2004, 25 Apr 2004 - 30 Apr 2004, Nice (France).

Nussbaumer, C. M., Crowley, J. N., Schuladen, J., Williams, J., Hafermann, S., Reiffs, A., Axinte, R., Harder, H., Ernest, C., Novelli, A., Sala, K., Martinez, M., Mallik, C., Tomsche, L., Plass-Dülmer, C., Bohn, B., Lelieveld, J., & Fischer, H. (2021). Measurement report: Photochemical production and loss rates of formaldehyde and ozone across Europe. Atmos. Chem. Phys., 21(24), 18413-18432. https://doi.org/10.5194/acp-21-18413-2021

Polinowski, V. (2023). Aufbau und Einsatz eines on-board Messsystems zur Untersuchung der Abgaszusammensetzung von Fahrzeugen betrieben mit konventionellen und alternativen Kraftstoffen RWTH Aachen (phD thesis, submitted).

Polinowski, V., Wegener, R., & Klemp, D. (2022). Luftchemische Bewertung alternativer Energieträger. In Bewertung des Einsatzes und der Auswirkungen alternativer Kraftstoffe für die Entwicklung der zukünftigen regionalen Infrastruktur - Abschlussbericht Kompetenzzentrum Virtuelles Institut – Strom zu Gas und Wärme (Vol. Band III, pp. 250-311). Virtuelles Institut - Strom zu Gas und Wärme. http://strom-zu-gas-und-waerme.de

Samad, A., Kiseleva, O., Holst, C. C., Wegener, R., Kossmann, M., Meusel, G., Fiehn, A., Erbertseder, T., Becker, R., Roiger, A., Stanislawsky, P., Klemp, D., Emeis, S., Kalthoff, N., & Vogt, U. (2023). Meteorological and air quality measurements in a city region with complex terrain: influence of meteorological phenomena on urban climate [Early Acess Article]. Meteorol. Z. (Contrib. Atm. Sci.)(07). https://doi.org/10.1127/metz/2023/1124

Schädler, G., & Lohmeyer, A. (1996). Kaltluft- und Windfeldberechnungen für Stuttgart (Untersuchungen zur Umwelt "Stuttgart 21", Issue 1).

Schneider, J., Kirchner, U., Borrmann, S., Vogt, R., & Scheer, V. (2008). In situ measurements of particle number concentration, chemically resolved size distributions and black carbon content of traffic-related emissions on German motorways, rural roads and in city traffic. Atmospheric Environment, 42(18), 4257-4268. https://doi.org/10.1016/j.atmosenv.2008.01.014

Talke, A., Misz, U., Konrad, G., Heinzel, A., Klemp, D., & Wegener, R. (2018). Influence of urban air on proton exchange membrane fuel cell vehicles - Long term effects of air contaminants in an authentic driving cycle [Article]. Journal of Power Sources, 400, 556-565. https://doi.org/10.1016/j.jpowsour.2018.08.063

Urban, S. (2010). Charakterisierung der Quellverteilung von Feinstaub und Stickoxiden in ländlichem und städtischem Gebiet,phD thesis, Univ. Wuppertal. Jülich. https://juser.fz-juelich.de/record/12159/files/Energie%26Umwelt_84.pdf

Wenk, A.-K. (2016). Optimierung und Anwendung eines schnellen GC-MS-Systems für mobile Messungen flüchtiger organischer Substanzen,phD thesis, University of Cologne. Cologne. https://kups.ub.uni-koeln.de/6877/1/Wenk_A_K_2016_Promotion.pdf

5 List of figures

6 List of tables

7 Abbreviations

3DO+M	Three-dimensional observation and modeling of atmospheric processes in cities
ALASKA	Evaluation of Air Emission Scenarios for the design of air filters and cathode regeneration cycles for automobile fuel cells
BMBF	Bundesministerium für Bildung und Forschung
BMWi	Bundesministerium für Wirtschaft und Energie
CAPS	Cavity Attenuated Phase-shift Spectroscopy
CBM	Carbon Bond Mechanism
CEST	Central European Standard Time
COSMO	COnsortium for Small-scale MOdelling
CPC	Condensation Particle Counter
CTM	Chemical Transport Model
DLR	Deutsches Zentrum für Luft- und Raumfahrt
DWD	Deutscher Wetterdienst (German Weather Service)
ECHO	Emission and CHemical transformation of biogenic volatile Organic compounds
ELPI:	Electrical Low Pressure Impactor
EU	European Union
EURAD-IM	EURopean Air pollution Dispersion – Inverse Model
EVA	Evaluation of Emission Calculation Models
FZJ	Forschungszentrum Jülich GmbH
GC	Gas Chromatography
HU	Humboldt University
IEK	Institute for Energy and Climate Research
IMK-IFU	Institut für Meteorologie und Klimaforschung - Atmosphärische Umweltforschung
IOP	Intensive Observation Period
IVLZ	Integrierte Verkehrsleitzentrale
KIT	Karlsruhe Institute for Technology
LES	Large eddy simulation
LTO	Long term observation
MCM	Master Chemical Mechanism
MOBINET	Mobility in the Munich Agglomeration
MOZAIK	Model-based city planning and application in climate change
PEGASOS	Pan-European Gas-AeroSols-climate interactiOn Study
PSS	Photostationary State
SCR	Selective Catalytic Reduction
TG	Trace Gas

TP	Teilprojekt (Subproject)
TU	Technical University
[UC2]	Urban Climate under Change
UTC	Coordinated Universal Time
VALM	Model for Validation
VALR	Observation for Validation
VOC	Volatile Organic Compound

8 Acknowledgements

Band / Volume 609
**Mechanisches Verhalten von Polymer-Elektrolyt-Membran-
Elektrolysezellen und -Stacks**
S. Holtwerth (2023), x, 251 pp
ISBN: 978-3-95806-697-7

Band / Volume 610
Membrane Reactor Concepts for Power-to-Fuel Processes
H. Huang (2023), VI, 197 pp
ISBN: 978-3-95806-703-5

Band / Volume 611
**Deployment of Fuel Cell Vehicles in Road Transport and the
Expansion of the Hydrogen Refueling Station Network: 2023 Update**
R. C. Samsun, M. Rex (2023), i, 39 pp
ISBN: 978-3-95806-704-2

Band / Volume 612
**Behavior/performance of tungsten as a wall material
for fusion reactors**
M. Gago (2023), X, 120 pp
ISBN: 978-3-95806-707-3

Band / Volume 613
**Strategieentwicklung zur Umsetzung der Klimaschutzziele im
Verkehrssektor mit dem Fokus Kraftstoffe**
M. Decker (2023), ix, 243 pp
ISBN: 978-3-95806-714-1

Band / Volume 614
Joining of tungsten and steel for the first wall of a future fusion reactor
V. Ganesh (2023), xxx, 142, a-v pp
ISBN: 978-3-95806-715-8

Band / Volume 615
**Polluter group specific emission optimisation for regional air quality
analyses using four-dimensional variational data assimilation**
P. M. Backes (2023), xxi, 115 pp
ISBN: 978-3-95806-717-2

Band / Volume 616
**Effect of organic soil amendments on increasing soil N retention
and reducing N losses from agricultural soils**
Z. Li (2023), XI, 134 pp
ISBN: 978-3-95806-721-9

Schriften des Forschungszentrums Jülich
Reihe Energie & Umwelt / Energy & Environment

Weitere *Schriften des Verlags im Forschungszentrum Jülich* unter
http://wwwzb1.fz-juelich.de/verlagextern1/index.asp

JÜLICH
Forschungszentrum